2-26-2015

Thermal Fluctuations Tunneling in Doped Conjugated Polymers

Troy C. Stedman
University of South Florida, isurus33@gmail.com

Thermal Fluctuations Tunneling in Doped Conjugated Polymers

by

Troy Stedman

A thesis submitted in partial fulfillment
of the requirements for the degree of
Master of Science
Department of Physics
College of Arts and Sciences
University of South Florida

Major Professor: Lilia M. Woods, Ph.D.
George S. Nolas, Ph.D.
Julie P. Harmon, Ph.D.

Date of Approval:
February 26, 2015

Keywords: Thermoelectricity, Organic, Transport, Linear Response

ACKNOWLEDGMENTS

It is truly lucky to have the opportunity to receive a higher education. I am grateful for the opportunity I have been given and I am grateful for everyone who helped me along the way. I would like to greatly thank my friends and my entire family for supporting me throughout.

This work was done with gratitude to the National Science Foundation under Contract No-DMR-1400957.

TABLE OF CONTENTS

LIST OF TABLES

LIST OF FIGURES

ABSTRACT

The possibility of using conducting polymers as organic alternatives to widely used inorganic materials for thermoelectric (TE) applications has received much attention in the past few decades. Since conducting polymers are generally inefficient compared to inorganic TE materials, research into their underlying transport mechanisms is required to improve their efficiency. We use a model based on the effects of local thermal fluctuations to characterize the transport in conducting polymer composites. With this model, full linear responses for the current and electronic heat current are obtained. From these responses, the local temperature dependent conductivity, electronic contribution to the thermal conductivity, and Seebeck coefficient are extracted and related to those of the composite material through an effective medium theory. The resulting simple expressions for the TE transport properties are easy to use and can improve our understanding of transport in conducting polymers. An example of how to use the model is given for a parabolic tunneling barrier and comparisons to experimental data are also provided.

1. INTRODUCTION

1.1 Current Energy Challenges

The past few decades have seen a staggering increase in global energy demands. An estimate based on current energy trends and policies indicates a 37% increase in global energy consumption by 2040 as compared to the end of 2013 [1]. The three primary energy sources to meet these demands come from oil, natural gas, and coal, comprising about 70% of all current energy consumption [2,3] (see Fig. 1). It is well known that these fossil fuels are limited natural resources and constitute an ever-diminishing source of energy. In addition, fossil fuels contribute to the emission of greenhouse gases. Carbon dioxide, CO_2, is the primary greenhouse gas and accounts for the majority of greenhouse gas emissions by mass. For example, CO_2 accounted for approximately 82.5% of all greenhouse gas emissions in the U.S. in 2012 [4]. These drawbacks of fossil fuels have led to the pursuit of alternative and renewable sustainable energy sources.

Of all the alternative energy sources, hydropower and nuclear power are the most used. However, hydroelectricity is limited by the possible water sources available and although nuclear power is relatively safe [5], it is generally approached apprehensively. The remaining alternative energy sources came from renewable energy. Renewable energy sources accounted for a record contribution of nearly 3% of global energy consumption in 2013 [2]. One possible alternative energy source is through the use of thermoelectric devices, where heat is converted into electricity. Thermoelectric devices have the benefit of being powered purely by a temperature gradient. Heat energy is ubiquitous and it is not hard to imagine the usefulness of transforming this energy to be used as a power source.

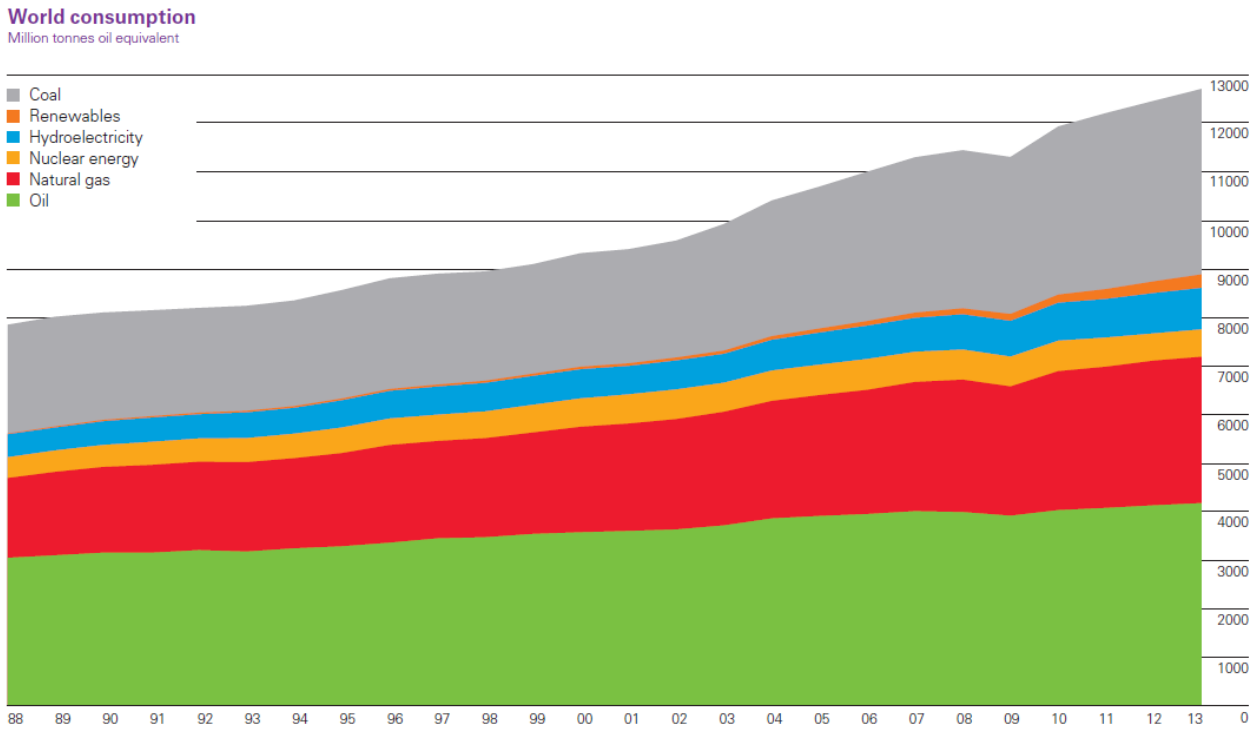

Figure 1. The world energy consumption from 1988-2013 in units of million tonnes of oil equivalent (MTOE) for different types of energy sources. The MTOE equates an amount of energy to the equivalent amount of energy released from burning the appropriate amount of oil. It is clear from the graph that oil, coal, and natural gas have remained the dominant sources of energy worldwide for the past couple of decades. This figure is reproduced from [2].

1.2 Thermoelectricity

In 1821, physicist Thomas Johann Seebeck conducted an experiment that demonstrated the deflection of a compass needle in the presence of a closed loop circuit made of two differing metal wires joined together at their ends when one of the contact junctions of the two metals is heated [6]. Seebeck conducted several later experiments in the 1820's that revolved around this observation [7,8]. He mistakenly concluded that the heat was directly affecting the compass needle magnetically. The correct explanation was given by the discoveries of physicist Hans Christian Ørsted who discovered that a current carrying wire gives rise to a magnetic field. With this observation, Seebeck's observations could be explained as follows: the deflection of the compass needle is due to the magnetic field of the current in the circuit loop caused by the temperature difference at the metal junctions. Seebeck's observations then led to the description of the general phenomena of a voltage being produced across a material as a result of a temperature difference across the material. Ørsted coined this as the "thermoelectric effect".

This phenomenon is also appropriately referred to as the "Seebeck effect" as there are other phenomena now collectively referred to as thermoelectric effects.

The "effectiveness" of a material in regards to the Seebeck effect is quantified in the Seebeck coefficient. The Seebeck coefficient (also known as the thermopower) S is defined as the negative of the ratio of the induced voltage difference ΔV (or corresponding electric field $\boldsymbol{E}$) produced across a material when a small temperature difference ΔT (or corresponding temperature gradient $\boldsymbol{\nabla T}$) is placed across the material:

$$S = -\frac{\Delta V}{\Delta T} \text{ (or equivalently } \boldsymbol{E} = -S\,\boldsymbol{\nabla T}\text{).} \tag{1.1}$$

The Seebeck coefficient S has SI units of volts/Kelvin. From these definitions, the Seebeck coefficient for a material can be found by measuring the voltage difference across the material when it has reached a steady-state with no net current in the material [9]. S can be either positive or negative, with positive S usually indicating holes as the charge carriers and negative S usually indicating electrons as the charge carriers.

Around 12 years after the findings of Seebeck, the French watchmaker and physicist Jean Charles Athanase Peltier discovered a related thermoelectric phenomenon. He found that a current passing through a circuit composed of two differing metal wires produces a temperature difference at the junction of the two wires [10]. Physicist Heinrich Friedrich Emil Lenz later expanded on Peltier's findings and showed that the junction of the wires can either heat up or cool down depending on the direction of the current [11]. This phenomenon is now appropriately referred to as the "Peltier effect" and describes the reversible flow of heat due to charge carriers constituting a current. Importantly, this effect is different than the irreversible effect of Joule heating [12].

In the Peltier effect, a heat current is produced in an isothermal material when there is an electric current. From this observation, the Peltier coefficient Π is defined by how much heat current $\dot{Q}$ is obtained for a given electric current I by

$$\dot{Q} = \Pi I. \tag{1.2}$$

The Peltier coefficient Π has SI units of volts.

A third thermoelectric effect is known as the Thomson effect, named after W. Thomson (also known as Lord Kelvin) who discovered this third thermoelectric effect while investing the thermodynamic relationships between the Seebeck effect and the Peltier effect [13]. When a current passes through a homogeneous material with an applied temperature difference, there is a reversible flow of heat due to the movement of the charge carriers constituting the current. This effect is known as the Thomson effect. The Thomson coefficient β is a material property that relates the heat current $\dot{Q}$ to the electric current I for small temperature differences ΔT by [14]

$$\dot{Q} = \beta I \Delta T. \tag{1.3}$$

The Thomson coefficient β has SI units of volts/Kelvin. Since the charge carriers are responsible for the transport of heat, the physical origin of the Thomson effect is the same as that of the Peltier effect.

Lord Kelvin's work also led him to the discovery of the relationships between all three thermoelectric effects. The relationship derived by Kelvin between the Peltier effect and Seebeck effect and their coefficients is given by

$$\Pi = TS, \tag{1.4}$$

where T is the uniform temperature throughout the material [9]. Also, the Thomson coefficient is related to the Seebeck coefficient by

$$\beta = T\frac{dS}{dT}. \tag{1.5}$$

These Kelvin relationships show that the Seebeck effect is the underlying physical effect behind the other thermoelectric effects [12]. Essentially, the Thomson effect is the Peltier effect throughout a material that has a temperature dependent Seebeck coefficient. The Thomson effect is generally of less importance in thermoelectric applications, but should not be ignored in careful considerations [14].

Thermoelectric coefficients are generally characterized by their relative values since the measurement of a physical quantity like current requires the formation of a junction between two dissimilar conductors, a thermocouple (Figure 2.). For a simple thermocouple, we have a relative Seebeck coefficient S_{AB}, relative Peltier coefficient Π_{AB}, and relative Thomson coefficient β_{AB} where A and B refer to the two dissimilar conductors (or materials) comprising the thermocouple. The relationships between these relative thermoelectric coefficients are given in terms of the difference between their absolute quantities for the materials of the thermocouple:

$$S_{AB} = S_A - S_B, \qquad \Pi_{AB} = \Pi_A - \Pi_B, \qquad \beta_{AB} = \beta_A - \beta_B. \tag{1.6}$$

These relationships give the thermoelectric coefficients for a thermocouple junction based on the thermoelectric coefficients of the materials comprising the thermocouple and rely on the assumption that the temperatures involved are not too small and that thermoelectric processes are reversible [12].

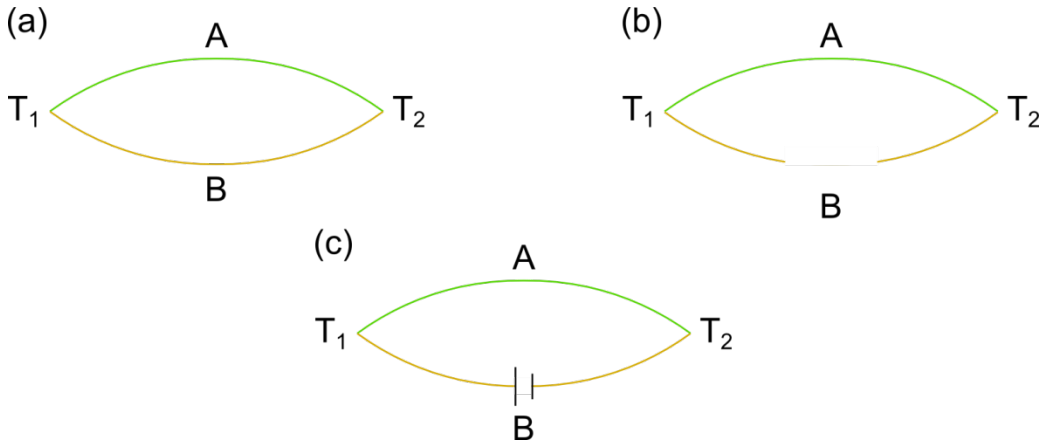

Figure 2. (a) A closed-circuit thermocouple with junctions at different temperature junctions subject to the Seebeck effect. The two materials are labeled A and B and the junctions of the thermocouple are at temperatures T_1 and T_2. (b) An open-circuit thermocouple with junctions at different temperatures. In the steady-state, the Seebeck effect will cause charge to

build up on the open-circuit ends until a voltage is produced, counteracting the Seebeck effect. (c) A thermocouple driven by a voltage, illustrating the Peltier effect at the thermocouple junctions.

The Peltier effect is actually defined in relation to a pair of dissimilar conductors connected to each other at their ends. If a current is passed through these joined conductors, the Peltier coefficient for this setup is the relative Peltier coefficient of the two conductors and we have the following relation between the heat current and electric current at the junctions of these two conductors, $\dot{Q} = \Pi_{AB}\mathrm{I}$. Heat is dissipated at one junction and an equivalent amount of heat is absorbed at the other junction (see Fig. 2).

Since practical measurements involve the formation of a junction between two dissimilar conductors or materials, the relative thermoelectric coefficients are more accessible. If the absolute thermoelectric coefficients of a material were 0, then the measurements of the relative thermoelectric coefficients of the thermocouple would give the absolute thermoelectric coefficients of the other material. Superconductors have thermoelectric coefficients of 0 and so could be used to establish the absolute thermoelectric coefficients of other materials. In practice, thermoelectric coefficients are generally given with respect to a reference. A common reference metal used is lead [13,14]. The Seebeck coefficient at higher temperatures can be extracted from the Kelvin relation between the Seebeck coefficient and the Thomson coefficient.

1.3 Thermoelectric Devices and Materials

Although the discoveries of thermoelectric effects in the early 1800's sparked considerable interest, interest waned in the late 1800's primarily due to the discoveries and advances in electromagnetism. In fact, it is only in the past 100 years that thermoelectricity has received serious attention towards application in devices [12]. During the 19th century and early 20th century, the thermoelectric materials available did not allow for useful energy conversion. It was the advent of

semiconductor technology in the 1950's that enabled thermoelectric principles to be used practically [13].

Thermoelectric devices primarily function from either the Seebeck effect for power generation or the Peltier effect for cooling applications. For power generation, a heat source and a heat sink are applied across a thermocouple or array of thermocouples, providing the required temperature difference. The thermocouples consist of two elements of dissimilar conductors connected at a junction on one end but separated at the conductor's other ends. This setup produces thermoelectric "legs" as seen in Figure 3. The load, the external device to be used, is then connected to these legs and a voltage is induced through the device from the voltage induced through the thermocouple by the Seebeck effect. For thermoelectric cooling, a dc (direct current) voltage source is connected to the legs instead of a load and the resulting current through the thermocouples pumps heat from one end of the thermocouple to the other.

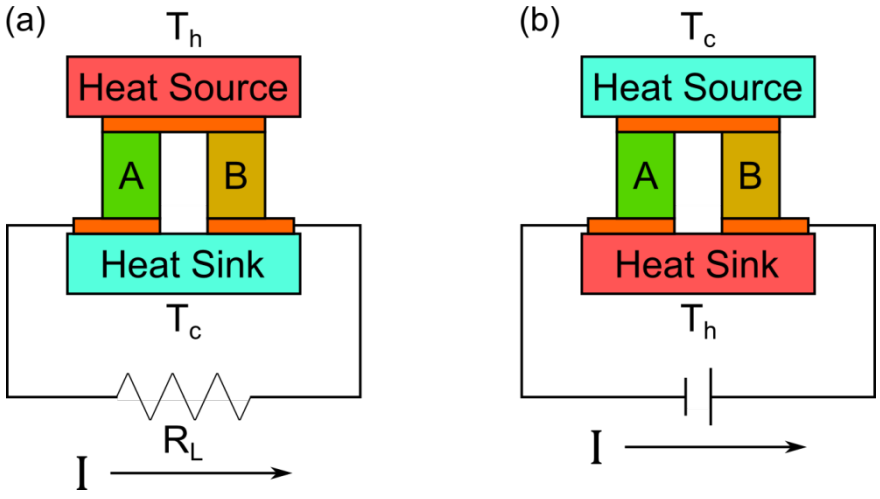

Figure 3. (a) A simple thermoelectric generator composed of a single thermocouple made up of materials A and B with a heat source at temperature T_h and a heat sink at temperature T_c. Because of the Seebeck effect, there is a current I through the external load with resistance R_L. (b) A simple thermoelectric cooler composed of a single thermocouple made up of materials A and B with a heat source at temperature T_c and a heat sink at temperature T_h. Because of the Peltier effect, the provided current I causes heat to leave the colder heat source reservoir and flow into the hotter heat sink.

Normally, thermoelectric devices require an array of thermocouples. The array of thermocouples is referred to as a thermoelectric module. The thermoelectric modules found in

thermoelectric devices are generally composed of many thermocouples connected electrically in series and thermally in parallel [13].

One of the most important aspects of a device in general is its performance. For thermoelectric generators, this would refer to the efficiency η of the generator and for thermoelectric coolers, this would refer to the coefficient of performance ϕ (COP). These devices operate as heat engines when generating electricity and refrigerators when operating as coolers. The efficiency of a heat engine and the coefficient of performance of a refrigerator are defined respectively as (e.g. [15])

$$\eta = \frac{Energy\ delivered\ across\ load}{Heat\ absorbed\ at\ hot\ reservoir} \quad \text{and} \quad \phi = \frac{Heat\ rejected\ at\ cold\ reservoir}{Work\ done\ in\ one\ cycle}. \tag{1.7}$$

Current thermoelectric devices have found niche functions as energy sources like in thermoelectric power generators in satellites. This is mainly because of the fact that thermoelectric devices have an inherently low efficiency.

Standard expressions for the maximum efficiency of a thermoelectric generator and the maximum coefficient of performance for a thermoelectric cooler based on a single thermocouple can be obtained if heat loss through conduction, convection, and radiation to the environment are ignored [13]. Furthermore, for these expressions, it is assumed that the thermal and electrical resistances between the thermocouples and the hot and cold junctions are negligible as compared to the thermal and electrical resistances of the thermocouple legs [14]. The electrical resistance R, thermal conductance K, and Seebeck coefficient S of the thermocouple are assumed to be independent of temperature as well so that the Thomson effect can be ignored. Under these assumptions, it is found that the efficiency η of a single thermocouple thermoelectric generator is given by

$$\eta = \frac{I^2 R_L}{K(T_1 - T_2) + (S_A - S_B) I T_1 - I^2 R/2}, \tag{1.8}$$

with the current

$$I = \frac{(S_A - S_B)(T_1 - T_2)}{(R + R_L)}. \tag{1.9}$$

Here the electrical resistance of the thermocouple is the resistances of the thermocouple legs in series:

$$R = R_A + R_B. \tag{1.10}$$

The resistances of the legs are related to the dimensions of the legs and the resistivity of the legs by

$$R_A = \frac{\rho_A L_A}{A_A} \quad \text{and} \quad R_B = \frac{\rho_B L_B}{A_B}, \tag{1.11}$$

where ρ_A (ρ_B) is the resistivity, L_A (L_B) is the length, and A_A (A_B) is the cross-sectional area of leg A (B) [15]. The length and cross-sectional area of the legs can be adjusted by changing its dimensions, but the resistivity is a material property of the legs that describes the resistance of the legs to produce a current under the influence of an electric field, like the viscosity of a fluid under the influence of a stress.

Also, the thermal conductance of the thermocouple is the thermal conductances of the thermocouple legs in parallel:

$$K = K_A + K_B. \tag{1.12}$$

The thermal conductances of the legs are related to the dimensions of the legs and the thermal conductivity of the legs by

$$K_A = \frac{\kappa_A A_A}{L_A} \quad \text{and} \quad K_B = \frac{\kappa_B A_B}{L_B}, \tag{1.13}$$

where κ_A (κ_B) is the thermal conductivity of leg A (B). The thermal conductivity is a material property of the legs that describes how easily the legs produce a heat current (flow) under the influence of a temperature difference.

The efficiency is a function of the load resistance. When the load resistance is chosen optimally, the efficiency is maximized yielding a maximum possible efficiency η_{max}:

$$\eta_{max} = \eta_C \frac{\sqrt{1 + Z\bar{T}} - 1}{\sqrt{1 + Z\bar{T}} + T_c/T_h}, \tag{1.14}$$

where $\eta_C = \frac{T_h - T_c}{T_h}$ is the Carnot efficiency [16], T_c and T_h are the temperatures of the cold and hot ends respectively, and $Z\bar{T}$ is the dimensionless figure of merit of the device with $\bar{T} = \frac{T_c + T_h}{2}$. The figure of merit Z has units of inverse temperature and is given by

$$Z = \frac{(S_A - S_B)^2}{KR}. \tag{1.15}$$

The load resistance in this case of maximum efficiency is

$$R_L = R(1 + Z\bar{T})^{1/2}. \tag{1.16}$$

It is clear that the maximum efficiency can be obtained by increasing the dimensionless figure of merit $Z\bar{T}$. This feature is also seen in the coefficient of performance for a thermoelectric cooler.

With the same assumptions as those for the thermocouple thermoelectric generator, the thermocouple can be driven by an externally supplied current I to provide a cooling mechanism. The coefficient of performance for the thermocouple cooler is then found to be

$$\phi = \frac{(S_A - S_B)IT_1 - K(T_2 - T_1) - I^2R/2}{(S_A - S_B)I(T_1 - T_2) + I^2R}. \tag{1.17}$$

The coefficient of performance is a function of the supplied current I. When the current is chosen optimally, the coefficient of performance is maximized yielding a maximum possible coefficient of performance ϕ_{max}:

$$\phi_{max} = \frac{T_c}{T_h - T_c}\frac{\sqrt{1 + Z\bar{T}} - T_h/T_c}{\sqrt{1 + Z\bar{T}} + 1}. \tag{1.18}$$

We would like to increase the maximum coefficient of performance and so, just like the case of the thermoelectric generator, we would like to increase $Z\bar{T}$.

Now, $Z = \frac{(S_A - S_B)^2}{KR}$ and $R = R_A + R_B = \frac{\rho_A L_A}{A_A} + \frac{\rho_B L_B}{A_B}$ and $K = K_A + K_B = \frac{\kappa_A A_A}{L_A} + \frac{\kappa_B A_B}{L_B}$. To maximize Z, the product KR needs to be minimized, but this product depends on the dimensions of the

thermocouple legs. When the respective dimensions of the thermocouple legs are identical, the product KR can be minimized giving

$$Z = \frac{(S_A - S_B)^2}{[(\rho_A \kappa_A)^{1/2} + (\rho_B \kappa_B)^{1/2}]^2}, \tag{1.19}$$

only dependent on the material properties ρ and κ of the thermocouple legs. This figure of merit is further simplified in special cases in which the legs have identical resistivities and thermal conductivities, but Seebeck coefficients opposite only in sign (that is, $S_A = -S_B$). This case is encountered, for example, with two semiconductors for legs that are identical in nature except one is p-type and the other is n-type. In the situation described above, the figure of merit Z simplifies to

$$z = \frac{S^2}{\rho\kappa}, \tag{1.20}$$

which is just the figure of merit z of both materials. This figure of merit is commonly rewritten as

$$z = \frac{\sigma S^2}{\kappa}, \tag{1.21}$$

where $\sigma = \frac{1}{\rho}$ is the conductivity of the materials given by Ohm's Law, $\boldsymbol{j} = \sigma \boldsymbol{E}$ for a current density $\boldsymbol{j}$ in the presence of an electric field $\boldsymbol{E}$ (e.g. [17]). Materials with a high conductivity produce large currents even for small voltages. This is the commonly cited figure of merit, but is only useful in the situation described above or when one of the legs is made up of a superconductor. Fortunately, in many situations the figure of merit Z of the thermocouple is approximately given by the average of the figure of merits z of the materials involved so that it can be useful to refer to the figure of merit z of a material as the quantity that should be maximized [13,14].

To maximize z, thermoelectric materials have a large Seebeck coefficient, and high conductivity but a low thermal conductivity. The fact that optimal thermoelectric devices need to have these special properties was first realized by Edmund Altenkirch who published his work on thermoelectric generators and coolers in 1909 and 1911 [18,19]. Materials with such properties

constitute a special class of materials since the thermal conductivity is frequently related to the conductivity. For example, metals have high conductivity and thermal conductivities while plastics have low conductivity and thermal conductivities. On the other hand, semiconductors have a relatively large conductivity, reasonable thermal conductivity, and a relatively large Seebeck coefficient so that semiconductors have a better z than that of metals and insulators. For this reason, many inorganic thermoelectric materials are semiconductors or based on semiconducting materials.

There are many types and classes of thermoelectric materials. As an example, Bi_2Te_3 is the best bulk inorganic thermoelectric material with $zT \sim 1$ at 300K (T is the temperature). Inorganic thermoelectric materials have several drawbacks including the scarcity of their constituents in nature, difficult and expensive synthesis processes, and their toxicity. Because of these drawbacks, there has been a pursuit in recent decades towards organic thermoelectric materials in the form of conducting polymers.

Conducting polymers as thermoelectric materials have several advantages over inorganic thermoelectric materials. In particular, the constituents of conducting polymers are abundant in nature, the polymers themselves are easy to synthesize with cost-effective processes, and are also nontoxic.

1.4 Conducting Polymers

Polymers are macromolecules formed by repeated subunits, monomers, chemically linked together to form a chainlike structure. Carbon is the element commonly constituting the basis of the monomer and sigma bonding between the carbons of neighboring monomers forms the backbone of the polymer, making most polymers organic. The carbon atoms in a polymer chain can either be sp^3 hybridized or sp^2 hybridized, described as saturated and conjugated respectively. In saturated polymers, only covalent σ bonds are present between neighboring monomers and a large band gap is formed between the σ bands. In conjugated polymers, one of the four valence 2p electrons of each carbon has

an electronic density perpendicular to the polymer backbone. The overlap of these neighboring 2p electrons leads to the formation of π orbitals and a delocalized electronic density. These π orbitals therefore have a band gap between the valence π band and the conduction π^* band that is much lower, on the order of 1-4 eV, than that of their o band counterparts in saturated polymers. Conjugated polymers are thus commonly semiconductors or insulators and make up an important class of conducting polymers.

There is a wide variety of different kinds of conducting polymers, like charge transfer polymer complexes, ionically conducting polymers, and conductively filled polymers [20], but we will focus on organic conjugated conducting polymers. Some examples of common organic conducting polymers used in thermoelectric applications include polyacetylene (PA), polyaniline (PANI), polypyrrole (PPY), poly(3,4-ethylenedioxythiophene) (PEDOT), polythiophene (PTH), and polycarbazoles (PC). Mixes of polymer blends are also possible, as in the case of poly(3,4-ethylenedioxythiophene): poly(sytrenesulfonate) (PEDOT:PSS). Figure 4 shows the chemical structure of some of these polymers.

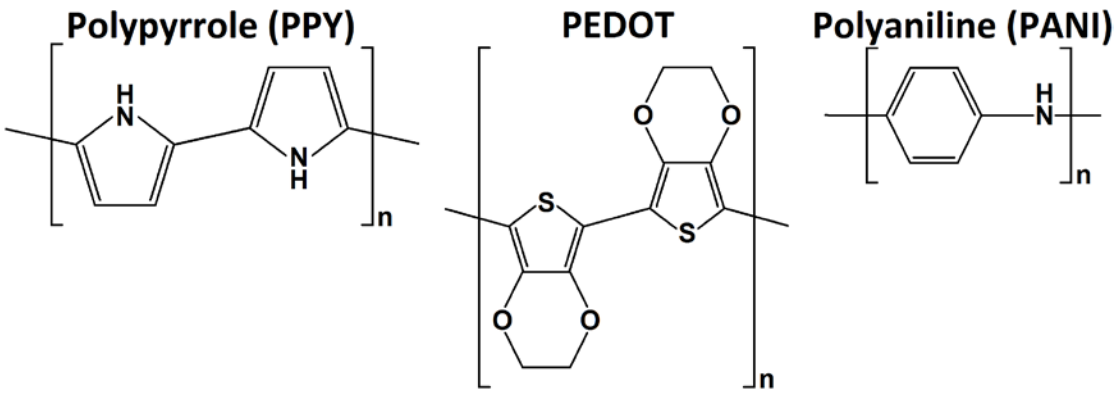

Figure 4. The chemical structure of some select polymers.

The conductivity of conjugated polymers is rather small due to the inherently low number of charge carriers. Proper doping of conjugated polymers can simultaneously significantly increase the number of charge carriers and decrease the π band gap, causing a large increase in conductivity. The effects of chemical doping of conjugated polymers were first observed in 1976 with polysulfur nitride

$(SN)_x$ [21] and in 1977 with polyacetylene [22] with a redox reaction governing the doping process in both cases. In the case of polyacetylene, it was found the conductivity can increase by many orders of magnitude (from 10^{-5} to 10^{2} S/cm). This drastic discovery was rewarded with a Nobel Prize in chemistry for 2000 to Alan J. Heeger, Alan McDiarmid, and Hideki Shirakawa for their work in the chemical doping of polyacetylene in 1977. Other conjugated polymers exhibit similar increases in conductivity upon doping and the formation of conducting polymers had been realized.

Doping in conjugated polymers is quite different than doping in inorganic semiconductors. There are different doping techniques for conjugated polymers, but doping usually results in much higher parts per million (ppm) doping levels. For example, doping in semiconductors is on the order of 1% or less ppm whereas doping in conducting polymers is typically several percent and can even be up to 35% [23]. Several doping techniques are possible, including chemical doping, electrochemical doping, photo-doping, charge-injection doping, and non-redox doping [20]. We will focus on chemical doping and electrochemical doping since the other doping methods do not introduce "counterions" to maintain an increase in the number of charge carriers.

In chemical doping, the conjugated polymer is exposed to either a gas or solution containing a redox agent. This doping agent is an electron acceptor/donor that acts as an oxidizing/reducing agent to reduce/oxide the conjugated polymer, resulting in p-type/n-type doping [20]. With this doping technique, the reduced/oxidized dopant becomes a counterion (anion/cation) of the polymer, neutralizing the deficit/excess charge from the doping redox reaction. NH_3 is an example of a reducing agent and I_2 is an example of an oxidizing agent used in chemical doping. An interesting feature of chemical doping is that most conjugated polymers have both possible reducing and oxidizing agent candidates [20]. Conductivities of conjugated polymers generally increase as the doping level increases, but eventually reach a saturation limit even as doping level increases. Furthermore, it was discovered

that an oxidizing agent can be used to counteract a reduced polymer in regards to the conductivity [24]. This allows for reversibility of changes in the electrical properties of a conducting polymer upon doping and enables potential tunability of the conducting polymer.

Electrochemical doping consists of immersing a conjugated polymer in an electrolyte solution containing the dopant and supplying an electric potential across the polymer with electrodes [23]. In this case, the polymer is in contact with one of the electrodes. The counterions are supplied by the electrode and oxidation/reduction is achieved when the electrochemical potential reaches the ionization energy/electron affinity of the polymer [23]. Compared to chemical doping, electrochemical doping has the advantage of providing simple, precise, and reversible control of the doping level through control of the current provided [20].

Since doped conjugated polymers are generally insoluble, techniques have been developed that lead to better organization of the polymer chains. These techniques are referred to as "secondary" doping to distinguish them from chemical and electrochemical doping that introduce counterions into the polymer. Secondary doping techniques increase the solubility of the doped conjugated polymers using dispersion of the polymer in high boiling point solvents with either soluble counterions or ionic surfactants [23]. This dispersion technique leads to better polymer chain organization and can greatly increase the conductivity.

The main function of the above processes is to increase the conductivity σ of conjugated polymers. This is useful in regards to thermoelectrics, but the Seebeck coefficient S should be large and the thermal conductivity κ should be small to maximize the possible use of conjugated conducting polymers for thermoelectricity.

Doped conjugated conducting polymers can exhibit drastically different conducting properties. For example, the range of conductivities can vary greatly and the conductivity can frequently

be anisotropic [25]. In the extreme case of polyacetylene doped through a redox reaction with I_2 vapors, the conductivity can fall in a range from 10^{-9}-10^5 S/cm [26-28]. However, in most conducting polymers, the range for the conductivity falls between 0.1-1000 S/cm with the highly conducting polymers having a conductivity of several hundred S/cm [29].

The conductivity of a conducting polymer can either be metallic or semiconducting in nature in regards to its temperature dependence [29]. For metallic conduction, the low temperature conductivity does not vanish, but remains finite whereas the low temperature conductivity vanishes for semiconducting conduction due to the lack of thermal energy required for charge carriers to traverse the band gap. Generally speaking, the nature of the conductivity is more semiconducting for low doping levels and becomes more metallic as the doping level increases [29].

Even though the temperature dependence of the conductivity can exhibit a metallic or semiconducting nature at low temperatures, the conduction processes is drastically different in polymers than conventional inorganic metals and semiconductors. The two major differences lie in the charge carriers responsible for the transport and the amorphous disordered polymer chain structure inherent in conducting polymers that is unlike the crystalline structure of metals and semiconductors. Both of these differences are discussed in more detail in the next section.

Although improving σ is beneficial for thermoelectrics, an increase in σ through doping usually comes at a cost of decreasing S [30]. Just like the conductivity, S has a wide possible range of values as well, varying between 10-1000 μV/K [31]. However, highly doped conducting polymers frequently have a thermopower less than 14 μV/K [23,29]. The sign of the thermopower is usually positive in polymers, indicating the charge carriers are predominantly holes [29]. Moreover, the sign of the thermopower can be positive even if a polymer is n-doped with electron donors [32].

Increasing the doping level decreases the magnitude of the thermopower and also changes its temperature dependence. For small doping, the thermopower is large and increases nonlinearly with temperature. For large doping, the thermopower is smaller but increases linearly with temperature [23,29]. The linear increase with temperature is typical of metallic behavior and suggests that a description of the thermopower in terms of metallic diffusion is valid (e.g. [9]). Lastly, the disorder in conducting polymers that greatly affects the conduction process does not significantly influence the thermopower [25].

Unlike the thermopower, the disorder in conducting polymers greatly impacts the thermal conductivity. In general, the thermal conductivity κ is composed of two parts, $\kappa = \kappa_e + \kappa_L$ where κ_e is the contribution to the thermal conductivity due to electrons (or holes) and κ_L is the lattice contribution to the thermal conductivity due to phonons. This is because, in general, both electrons/holes and phonons can transport heat. In conducting polymers, phonon transport is the dominant contribution to the thermal conductivity [23]. The amorphous, disordered structure of conducting polymers limits phonon transport and therefore greatly reduces the thermal conductivity. As a result, conducting polymers have much lower thermal conductivities than crystalline metals and semiconductors.

The Wiedemann-Franz law relates κ_e to σ for a material at temperature T by $\frac{\kappa_e}{\sigma} = LT$ where $L = \frac{\pi^2}{3}\left(\frac{k_B}{e}\right)^2 = 2.44 \times 10^{-8}\ W \cdot \Omega \cdot K^{-2}$ is the Lorenz number. This model assumes a free electron gas model for the charge carriers and is generally valid or approximate for many materials in the low and high temperature ranges (a few Kelvin and above hundreds of Kelvin), but not in intermediate temperature ranges [9]. For metals, the dominant carriers of heat come from charge carriers and the Wiedemann-Franz law can give a good approximation to the total thermal conductivity. It is believed and has been observed that the Wiedemann-Franz law does not hold for polaron and bipolaron charge carriers and that there is a strong temperature dependence of the Lorenz number [33].

Although there have not been substantial thermal conductivity measurements of conjugated conducting polymers, these polymers usually have a thermal conductivity lower than some of the best known thermoelectric materials [23,30,31,34]. The thermal conductivity of conducting polymers can fall in the range 0.02-1 W/m·K, with most conducting polymers having a thermal conductivity between 0.2-0.7 W/m·K. For comparison, Bi_2Te_3 has a thermal conductivity of 1.4-2.4 W/m·K [23,31]. Like the conductivity, the thermal conductivity can also be anisotropic due to the alignment of the polymer chains [23].

Unfortunately, despite the reasonable conductivity and Seebeck coefficient and lower thermal conductivity than the best thermoelectric materials, the figure of merit zT is inferior compared to the best inorganic thermoelectric materials. Most conducting polymers have a zT between $10^{-4} - 0.1$ at room temperature [34]. By careful control of the doping level and secondary doping with high boiling point solvents, PEDOT can obtain a zT between $0.25 - 0.42$ at room temperature[35,36]. Bi_2Te_3 alloys on the other hand can obtain a very large figure of merit, with a measured $zT = 1.4$ at room temperature [37].

Table 1. shows a compilation of the transport properties and their wide range of values for various polymers. Some maximum measured figures of merit are also included.

Table 1. Observed ranges of the conductivity, Seebeck coefficient, thermal conductivity for select conducting polymers. Some figures of merit are also included. The values shown are a collection for polymers that are prepared differently and with different doping processes and doping levels. All data was reproduced from [34].

Polymer	$\boldsymbol{\sigma}$ $\mathbf{(S/cm)}$	$\mathbf{S}$ $\boldsymbol{(\mu V/K)}$	$\boldsymbol{\kappa(W/m \cdot K)}$	$\mathbf{zT_{max}}$ $\mathbf{(Temperature)}$
PANI	$10^{-7} - 320$	$-16 - 225$	$0.02 - 0.542$	1.1×10^{-2} $(423K)$
PEDOT:PSS	$0.06 - 945$	$8 - 888$	0.34	1×10^{-2} $(300K)$
PPY	$0 - 340$	$-1 - 40$	0.2	0.1 (Room Temp)
PTH	$10^{-2} - 10^{3}$	$10 - 100$	$0.028 - 0.17$	2.9×10^{-2} $(250K)$
PA	$1.53 \times 10^{-3} - 2.85 \times 10^{4}$	$-0.5 - 1077$	–	–
PC	$4 \times 10^{-5} - 500$	$4.9 - 600$	–	–

Despite all of the experimental measurements and data collection of the transport properties of conducting polymers, there is still an incomplete understanding of the transport mechanisms involved in conducting polymers. To improve conducting polymers for thermoelectrics, it is necessary to have a better understanding of these transport mechanisms. The main objective of this work is to outline a complete transport model in conjugated conducting polymers for thermoelectrics that allows characterization of the conductivity, the electronic thermal conductivity, and the Seebeck coefficient.

2. TRANSPORT IN CONDUCTING POLYMERS

2.1 Description of Transport

The π orbitals in conjugated polymers form the basis for electron/hole transport. Solid state band theory (e.g. [9]) is commonly used to describe the transport in conjugated polymers with the bands formed from the transverse π bonds along the polymer backbone. With this theory, electrons/holes can traverse the polymer through these bands. However, doping of conjugated polymers leads to a scenario where the charge carriers are not simply described by electrons/holes.

In band theory, a crystalline lattice leads to the formation of discrete energy levels (a specific set of these energy levels constitutes a band) which the electrons inhabiting the lattice must occupy starting from the lowest energy level and obeying the Pauli exclusion principle. As a consequence, the bands of the lattice may be either partially filled or completely filled in addition to other bands being empty, depending on the lattice itself. If there are partially filled bands, the highest occupied energy level is referred to as the Fermi energy and lattices with this configuration have metallic properties. In the case where some bands are completely filled with all the rest remaining empty, then we have a different scenario. Here, there is an energy difference between the highest occupied energy level of the filled band and the lowest occupied energy level of the empty band. This energy difference is referred to as a band gap. In order for electrons to propagate through a lattice with this band structure, electrons in the filled band (valence band) must obtain enough energy to surmount the band gap to reach the empty band (conduction band). Lattices with a large band gap are insulators and lattices with a small band gap are semiconductors.

For conjugated conducting polymers, the band theory approach commonly applied to inorganics is a good reference to describe the charge transport, but modifications must be made to account for doping. In addition to providing extra charge carriers (electrons/holes), the chemical and electrochemical doping processes of conjugated polymers lead to the formation of counterions within the polymers [20]. As a result, both the additional charge carrier and the counterion distort the surrounding polymer structure through Coulomb interactions. The polymer relaxes into an energetically favorable geometry, leading to a localized distortion. The distortion itself can extend over three to four monomers. Furthermore, two additional electronic levels appear in between the band gap: a level above the valence band and a level below the conduction band. These states are referred to as polaron states and the extra charge carrier (electron/hole) along with the accompanying localized distortion are referred to as a polaron [23]. Here, the charge is localized due to the distortion, instead of being delocalized across the polymer backbone as would be the case with no doping. Depending on the spatial extent of the polaron, polarons may be classified as small or large.

The electron that is either removed from the valence band or added to the conduction band upon doping occupies either the lower polaron state (closer to the valence band) or the upper polaron state (closer to the conduction band) so that the valence and conduction bands themselves remain full or empty respectively [38]. However, the polaron is a spin-1/2 quasi-particle and can either have positive or negative charge, depending respectively on whether a hole is in the lower polaron state from p-type doping or an electron is in the upper polaron state from n-type doping. A polaron with positive charge +e is called a positive polaron (radical cation) and a polaron with negative charge –e is called a negative polaron (radical anion) [39].

Upon further doping, a second polaron can be created with extra accompanying polaron states or an extra electron/hole can be added to the upper/lower polaron states. In the latter case,

there is further distortion of the polymer and a bipolaron is formed. A bipolaron is the pair of like charges formed from the process described along with the accompanying lattice distortion that is more pronounced than that of a single polaron and can extend over more monomers than a single polaron. A pair of two positive charges constitutes a positive bipolaron (closed-shell cation) with charge +2e and a pair of two negative charges constitutes a negative bipolaron (closed-shell anion) with charge -2e [39]. When a bipolaron is formed, the two polaron states move energetically closer as the lower polaron state moves upward and the upper polaron state moves downward. The two charges of a bipolaron occupy the same polaron state and bipolarons are therefore spinless by the Pauli exclusion principle. Finally, bipolarons are less stable than polarons and will split into polarons under the influence of an electric field so that charge transport is actually accompanied by polarons [40].

Charge carriers in conducting polymers can also manifest in a third form- a soliton. Solitons are only found in conducting polymers with two possible geometric structures (ground states) that are energetically identical [23]. These degenerate structures give rise to a soliton instead of a bipolaron. Conducting polymers with nondegenerate ground states produce polarons and bipolarons. Solitons can either have positive, negative, or neutral electric charge. Interestingly, a charged soliton is spinless but a neutral soliton has spin ½ [38]. For now, only trans-polyacetylene is characterized by soliton charge transport. This special case of soliton charge transport will not be considered in this work.

Besides the nature of the charges in conducting polymers, transport is drastically different than that of crystalline metals and semiconductors due to inherent disorder in the structure of conducting polymers. Conducting polymers can either be amorphous or semi-crystalline and disorder manifests through various properties of the polymer like the size of the crystalline domains, chain orientations, and inter-chain distance [23]. Long groups of aligned polymer chains are interrupted by regions where the chains becomes disordered, leading to many bounded crystalline regions that

together form the structure of the polymer (Fig. 5). Disorder affects charge transport in drastic ways and alters transport properties like the conductivity and Seebeck coefficient [25].

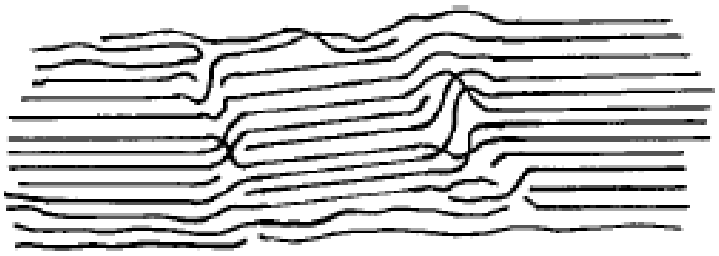

Figure 5. Crystalline regions of polymer chains interrupted by areas of disordered chain segments. This picture is reproduced from [29].

Conduction is generally inhibited due to disorder. Since the transport of charge carriers depends on the spatial extent of the polaron in relation to the characteristic size of the disorder, two cases emerge. If the spatial extent of the polarons exceeds the dimensions of the crystalline domains, homogeneous disorder is observed and electronic coupling between polymer chains is the main feature responsible for limiting the conduction. On the other hand, if the spatial extent of the polarons is less than that of the crystalline domains, the main factor limiting the conduction is the energy barrier the carriers encounter in between neighboring crystalline domains.

For highly doped conducting polymers, the limiting factor for conduction is expected to be the transport across the largest energy barriers encountered by the charge carriers since most of the energy landscape becomes smooth due to the large amount of doping. In this way, the polarons can form large regions that are metallic in nature due to the smooth energy landscape and transport is governed by the ability of charge carriers to traverse between these neighboring metallic regions. For this transport mechanism, the conduction process is similar to that of granular metals.

The charges involved in transport in conducting polymers have been identified and the disorder inherent in conducting polymers plays a vital role in the transport of such charges. However, the actual mechanism by which these charges traverse a polymer is still a matter of debate. There are

several models for the transport of charge, but we will focus on two common models: variable-range hopping and fluctuation-induced tunneling. The model present in this work focuses on fluctuation-induced tunneling.

2.2 Variable-Range Hopping

Phonon-assisted tunneling is a general mechanism thought to describe the transport of polarons and bipolarons in conducting polymers. Through this mechanism, phonons supply the polarons and bipolarons with enough energy to surmount any energy barriers between neighboring localized states throughout the polymer. This process is frequently referred to as "variable-range hopping", "Mott's variable-range hopping", or simply "hopping". Charge transport occurs as a polaron hops from one localized site to another. The hopping sites are greatly affected by the disorder in a conducting polymer.

Within this mechanism, the conductivity can be shown to have a temperature dependence given by (e.g. [41])

$$\sigma = \sigma_0 e^{-\left(\frac{T_0}{T}\right)^{\gamma}}, \tag{2.1}$$

with $\gamma = \frac{1}{D+1}$ where D is the dimensionality of the hopping. σ_0 has some temperature dependence, but the this temperature dependence is not agreed upon and is often disregarded because of the exponential factor. T_0 is a factor that depends on the localization length of the charge carriers and the localized density of states at the Fermi level.

An expression for the thermopower has also been derived for variable-range hopping. For constant density of states, the thermopower has a temperature dependence given by (e.g. [42])

$$S \propto \sqrt{T}. \tag{2.2}$$

For a nonconstant density of states, a different temperature dependence is obtained. However, the above power law, $T^{1/2}$, is commonly used. For example, in lightly doped conducting polymers, a temperature dependence similar to or given by this power law can be observed [23].

2.3 Fluctuation-Induced Tunneling

In this model, a disordered material consists of many microscopically large metallic conducting regions separated by insulating material [43]. The closest point of contact between neighboring conducting regions is small compared to the dimensions of the regions themselves at this junction. Associated with this junction is a potential energy barrier for the insulating material that makes up the junction. In the presence of an electric field across this junction, electrons can tunnel through this junction or hop over the junction giving rise to a net transport of electrons across the junction. Therefore, a means of charge transport is realized. This transport can be affected due to thermal fluctuations that can cause excess or deficit charge to build up on the junction faces, creating a local field across the junction. Due to the small width of the junction and large surface area of the conducting regions at the junction, we would expect these fluctuations and their associated induced fields to significantly alter the field across the junction even in the presence of an applied field. The significance of the junction thermally induced fields is the main principle of Sheng's fluctuation-induced tunneling model. The modifying effects of the thermally induced fields should then be statistically averaged over all possible thermally induced fields for observable transport responses and quantities.

Assuming a parabolic barrier in the insulating regions between the conducting regions, the temperature dependent conductivity is found to be

$$\sigma = \sigma_0 e^{-\left(\frac{T_1}{T+T_0}\right)}, \tag{2.3}$$

where σ_0 , T_0, and T_1 are constants and T_0 and T_1depend on the junction parameters.

Since highly doped conducting polymers exhibit conducting properties similar to that of granular metals, the fluctuation-induced tunneling model is readily applicable for these disordered systems with the transport occurring through the metallic regions of the polymer [44]. The presence of thermal fluctuations can modify the transport across these metallic regions in a manner described by fluctuation-induced tunneling. The purpose of this work will be to examine the effects of fluctuation-induced tunneling to determine the transport properties of highly doped conducting polymers.

3. MOTIVATION AND MODEL

3.1 Motivation

To improve the efficiency of thermoelectric devices, specific tuning of their transport properties can be useful. This tuning is especially important for thermoelectric devices where a large figure of merit is desired. For example, increasing the conductivity is generally accompanied by a decreasing thermopower and thus these effects on the figure of merit are unclear. An understanding of the transport processes involved in thermoelectric materials allows for easier tuning of transport properties. For conducting polymers, the transport processes involved are not fully understood. This lack of understanding is in part because there has been little investigation of these transport mechanisms due to the recent discovery of conducting polymers and the transport mechanisms in conducting polymers are generally more complicated than other commonly studied thermoelectric materials, like crystalline semiconductors. Variable-range hopping and fluctuation-induced tunneling are two models often used to describe the transport in conducing polymers. There has been more investigation of the variable-range hopping model than the fluctuations-induced tunneling model, where only the conductivity has been discussed.

The focus of our model is the fluctuation-induced tunneling model. Fluctuation-induced tunneling has proven to be a successful model for conduction in many composite material systems like carbon polyvinylchloride (C-PVC) [45], indium tin oxide nanoparticle films [46], graphene/(poly)vinyl alcohol composites [47], graphene nanoplatelets/polystyrene nanocomposites [48], carbon nanotubes [29,44,49], and various conductive polymers [29,44]. It is in light of this success that we revisit Sheng's model [43].

We present an analysis of the fluctuation-induced tunneling model that will include the electronic heat current and the linear responses to a temperature gradient. In doing so, we will have a complete linear transport theory for the electric and heat currents in the presence of an applied field and temperature gradient. This linear theory will then allow for characterization of thermoelectric parameters. There have been other extensions of Sheng's model [50-53], but none of them investigated current responses to temperature gradients or the electronic heat current itself.

3.2 Overview

To begin, a more thorough analysis of fluctuation-induced tunneling is needed. A disordered material, which conducting polymers mimic, consists of separated conducting regions dispersed in an insulating matrix. Transport of charge is mediated by tunneling through neighboring conducting regions. Most of the transport occurs through a junction formed at the closes point of contact between these regions. The transport is modified by thermal fluctuations that cause local fields in between the junction due to excess or deficit charge built up on the faces of the junction (Fig. 6). Because this local field fluctuates with no preferential effects, there is no net transport across the junction in the absence of an applied field. An applied field produces net transport in the direction of the field, but modified by the local fluctuating field.

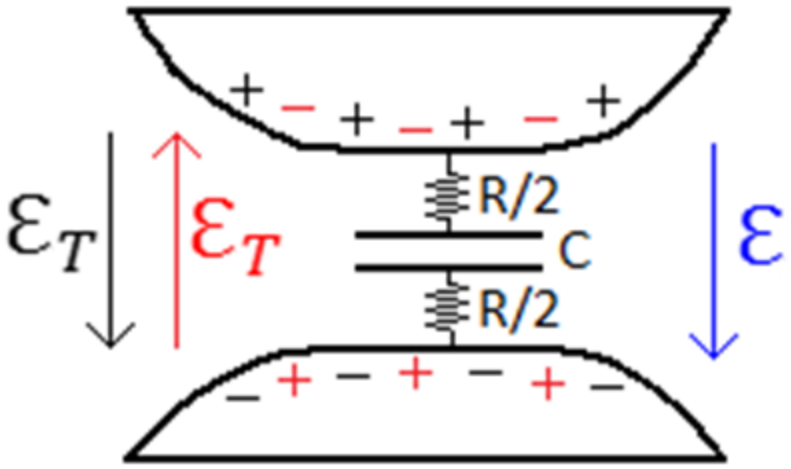

Figure 6. Schematic of a junction approximated by a parallel plate capacitor of capacitance C with resistances $R/2$ associated with the junction. A fluctuating field of strength $\mathcal{E}_T$ can point across the junction in either direction, depending on the accumulation of charge on the junction faces. Here there is also an external field $\mathcal{E}$ applied across the junction.

The junction itself is approximated as a parallel plate capacitor, whose plates are the faces of the neighboring conducting regions. The capacitor has a capacitance C and the junction has an associated resistance R, distributed equally on both sides of the capacitor plates. With this parallel plate capacitor model for the junction, Sheng showed that the fluctuation probability function follows a Boltzmann distribution:

$$P(\mathcal{E}_T) = \left(\frac{4a}{\pi kT}\right)^{1/2} e^{\left(-a\mathcal{E}_T^2/k_BT\right)} \quad \text{with} \quad a = \frac{\varepsilon_0 wA}{2}. \tag{3.1}$$

Here, w is the width of the junction, A is the area of the parallel plates comprising the junction, ε_0 is the permittivity of the insulating material in the junction, $\mathcal{E}_T$ is the fluctuation-induced field in between the junction, k is Boltzmann's constant, and T is the temperature of the reservoirs. This probability function gives the probability that a thermally induced field of strength $\mathcal{E}_T$ appears across the junction due to the charge fluctuations on the junction faces.

Any quantity $H(\mathcal{E}_T)$ that is dependent on the thermally induced field is averaged over the probability $P(\mathcal{E}_T)$ using the following

$$\langle H \rangle = \left(\frac{4a}{\pi k_B T}\right)^{1/2} \int_0^\infty H(\mathcal{E}_T) e^{\left(-a\mathcal{E}_T^2/k_BT\right)} \, d\mathcal{E}_T. \tag{3.2}$$

The presence of a temperature gradient also affects charge transport across the junction. An applied temperature difference across a disordered material will create local temperature gradients between neighboring conducting regions at different temperatures. Even in the absence of thermal fluctuations, a temperature gradient would lead to a net transport of charge. We would like to find the thermoelectric transport properties of a junction in the presence of thermal fluctuations. Transport across a junction in the presence of both a temperature gradient and electric field is an intrinsically nonequilibrium process. However, assuming the temperature gradient and electric field are both small, we can approximate the transport as a quasiequilibrium process. A small temperature difference between the junctions is a necessary assumption for the approach used here.

We will find linear expressions for both the current and heat current in terms of the applied field and temperature gradient. The heat current that we will be examining is strictly due to the transport of charge. Hence, the transport of heat due to phonons is neglected here.

Since the temperature difference between neighboring conducting regions is small, we make the crucial assumption that the dominant contribution to the fluctuations comes from the equilibrium Johnson-Nyquist noise. Because neighboring regions are separated by a much smaller distance than the dimensions of a composite material, a small applied temperature difference across the material leads to an even smaller difference in temperature across the regions. Hence, the assumption that the fluctuations are dominated by the equilibrium Johnson-Nyquist noise seems reasonable. A simple expansion of the equilibrium fluctuation probability in ΔT about temperature T gives the approximate fluctuation probability for small ΔT. All terms of order ΔT and higher in this fluctuation probability expansion give terms in the currents that are of second order. Therefore, the linear responses of the currents depend only on the equilibrium Johnson-Nyquist noise. Also, it was shown that the Johnson-Nyquist noise is dominant compared to the out of equilibrium noise for a tunneling

junction in the presence of an electric field and temperature gradient [54]. In this reference, contributions to the power spectrum due to out of equilibrium effects are also second order in ΔT.

3.2 Currents and Responses

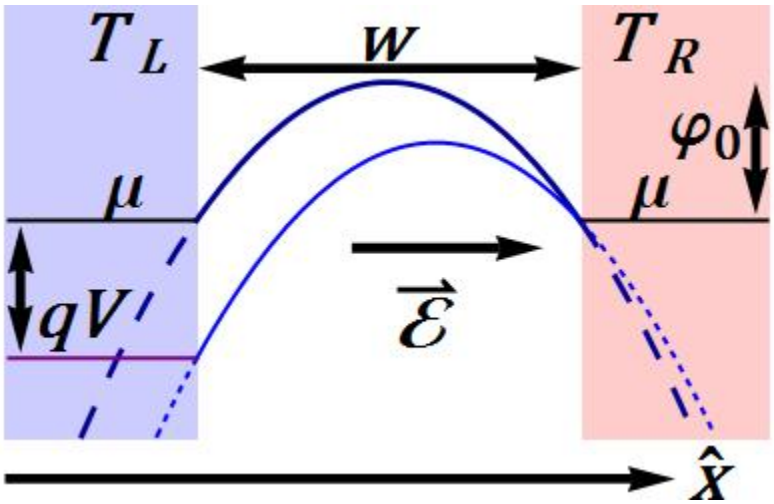

Figure 7. The extended parabolic barrier with barrier height φ_0 in a tunneling junction of width w. Dashed lines indicate the continuation of the barrier outside of the junction. The conducting region on the left is at a temperature T_L and a potential qV lower than the conducting region on the right due the electric field $\vec{\mathcal{E}}$ pointing to the right. The right reservoir is at temperature T_R. The chemical potential of the two conducting regions is μ.

The junction we will be analyzing will have one conducting region on the left and another conducting region on the right (Fig. 7). These two regions are at different potentials and temperatures, with the applied field across the junction and the temperature gradient both pointing to the right. For the currents, we use a Landauer expression [55,56]. The electric current and electronic heat current are then given respectively by

$$j = \frac{2q}{(2\pi)^3\hbar}\int dE_x d^2k_{||}\left[f_R - f_L\right]D(\mathcal{E}, E_x) \tag{3.3a}$$

and

$$j^q_{L,R} = \frac{2}{(2\pi)^3\hbar}\int dE_x d^2k_{||}[f_R - f_L]\left[E(\boldsymbol{k}) - \mu_{L,R}\right]D(\mathcal{E}, E_x). \tag{3.3b}$$

Here, q is the electronic charge, $\hbar$ is Planck's constant, $D(\mathcal{E}, E)$ is the tunneling probability with field $\mathcal{E}$, $f_R$and f_L are the Fermi functions for the right and left reservoirs respectively, and $\mu_R$and μ_L

are the Fermi levels for the right and left reservoirs respectively. For the heat current, the subscripts L and R refer to the heat current *entering* the left reservoir and *leaving* the right reservoir respectively. The only differences between these two reservoirs are the Fermi level in each of the reservoirs and their respective temperatures. The integration is over all possible longitudinal wave vectors $k_{||}$ for the charge carriers and from the bottom of the conduction band to infinity for the energy $E_x = \frac{\hbar^2 k_x^2}{2m}$ associated with the transverse tunneling of charge carriers (k_x is the transverse wave vector). However, we will use a common approximation to extend the lower limit of integration for E_x to minus infinity with little incurred error.

As the conducting regions are metallic in nature, we assume a free particle parabolic energy dispersion $E = \frac{\hbar^2 k^2}{2m} = \frac{\hbar^2 k_x^2}{2m} + \frac{\hbar^2 k_{||}^2}{2m} = E_x + \frac{\hbar^2 k_{||}^2}{2m}$ for the electrons, where k is the electron wave vector and m is the effective mass. In doing so, we can make a change of variables to express the currents using only integrations over energy:

$$j = 2\int_{-\infty}^{\infty} dE\big[f_R - f_L\big]M(\mathcal{E}, E). \tag{3.4a}$$

$$j_{L,R}^{q} = 2\int_{-\infty}^{\infty} dE[f_R - f_L]\big[E - \mu_{L,R}\big]M(\mathcal{E}, E). \tag{3.4b}$$

$$M(\mathcal{E}, E) = \frac{qm}{(2\pi)^2\hbar^3}\int_{-\infty}^{E} D(\mathcal{E}, E_x)dE_x. \tag{3.4c}$$

Since only the relative difference between Fermi levels is relevant here, we opt for a scheme that raises the Fermi level of the reservoir with lower potential and lowers the Fermi level of the reservoir with higher potential by equal amounts to ensure a drop in Fermi level across the junction equal to the potential difference between the reservoirs. This is equivalent to just shifting the energy upwards by $\frac{qV}{2}$ in Fig. 7. We ignore any temperature dependence in the chemical potential. This is a valid assumption for metals at room temperature and is therefore used for the metallic conducting regions of the model.

j_L^q and j_R^q are different due to the different Fermi levels of the reservoirs. The differing terms subsist in the linear response expansion of the currents but do not contribute to the linear responses. Furthermore, these terms exist in the full current expressions even in the absence of any applied field or temperature gradient and are specifically due to the differences in $\mu_{L,R}$ by $\mathcal{E}_T$. To remedy this, we discard all terms differing from j_L^q and j_R^q in their linear response expansions. In our scheme of raising the Fermi level of the lower potential reservoir and lowering the Fermi level of the higher potential reservoir, this amounts to averaging j_L^q and j_R^q to get the newly defined junction j^q of the junction.

$$j^q = \frac{j_L^q + j_R^q}{2}. \tag{3.5}$$

To thermally average the currents, we need to account for the two directions the fluctuating field can take. We must average the currents over the two possible field orientations in addition to averaging over the fluctuating field magnitudes $\mathcal{E}_T$. We also assume $\mathcal{E}_T > \mathcal{E}$ for the linear response.

$$\bar{j} = \frac{j(\mathcal{E}_T + \mathcal{E}, \nabla T) + j(\mathcal{E} - \mathcal{E}_T, \nabla T)}{2}. \tag{3.6a}$$

$$\bar{j}^q = \frac{j^q(\mathcal{E}_T + \mathcal{E}, \nabla T) + j^q(\mathcal{E} - \mathcal{E}_T, \nabla T)}{2}. \tag{3.6b}$$

Thermal averaging over the fluctuating field magnitudes $\mathcal{E}_T$ gives the currents

$$J = \langle \bar{j} \rangle, \tag{3.7a}$$

$$J^q = \langle \bar{j}^q \rangle. \tag{3.7b}$$

Under a linear response approximation, we have the currents and explicit forms for their responses:

$$J = \langle \mathcal{L}_{11} \rangle \mathcal{E} + \langle \mathcal{L}_{12} \rangle \nabla T. \tag{3.8a}$$

$$J^q = \langle \mathcal{L}_{21} \rangle \mathcal{E} + \langle \mathcal{L}_{22} \rangle \nabla T. \tag{3.8b}$$

$$\mathcal{L}_{11} = 2\frac{\partial L_1}{\partial \mathcal{E}_T}, \quad \mathcal{L}_{12} = w\frac{\partial L_2}{\partial T}, \quad \mathcal{L}_{21} = 2\frac{\partial L_1^q}{\partial \mathcal{E}_T}, \quad \mathcal{L}_{22} = w\frac{\partial L_2^q}{\partial T}. \tag{3.9}$$

$$L_1(\mathcal{E}_T, T) = \int_{-\infty}^{\infty} dE \left(f\left(E - \frac{ew\mathcal{E}_T}{2}, T\right) - f\left(E + \frac{ew\mathcal{E}_T}{2}, T\right) \right) M(\mathcal{E}_T, E). \tag{3.10a}$$

$$L_2(\mathcal{E}_T, T) = \int_{-\infty}^{\infty} dE \left(f\left(E - \frac{ew\mathcal{E}_T}{2}, T\right) + f\left(E + \frac{ew\mathcal{E}_T}{2}, T\right) \right) M(\mathcal{E}_T, E). \tag{3.10b}$$

$$L_1^q(\mathcal{E}_T, T) = \frac{1}{e}\int_{-\infty}^{\infty} dE \left(f\left(E - \frac{ew\mathcal{E}_T}{2}, T\right) - f\left(E + \frac{ew\mathcal{E}_T}{2}, T\right) \right) [E - \mu] M(\mathcal{E}_T, E). \tag{3.10c}$$

$$L_2^q(\mathcal{E}_T, T) = \frac{1}{e}\int_{-\infty}^{\infty} dE \left(f\left(E - \frac{ew\mathcal{E}_T}{2}, T\right) + f\left(E + \frac{ew\mathcal{E}_T}{2}, T\right) \right) [E - \mu] M(\mathcal{E}_T, E). \tag{3.10d}$$

3.3 No Fluctuations

To find the linear responses in the absence of fluctuations, we just need to replace the fluctuation probability with a delta function distribution. Specifically, we set

$$P(\mathcal{E}_T) = \delta(\mathcal{E}_T). \tag{3.11}$$

In doing this, the fluctuation probability function is a delta function located at zero for the fluctuating field so no fluctuating fields can appear across the junction. We will find the linear responses and transport quantities in the absence of fluctuations in addition to those in the presence of fluctuations.

3.4 Transport Quantities

With these responses, the conductivity, electronic thermal conductivity, and thermopower are defined respectively as

$$\sigma = \langle \mathcal{L}_{11} \rangle, \tag{3.12a}$$

$$\kappa_e = \langle \mathcal{L}_{22} \rangle - \frac{\langle \mathcal{L}_{12} \rangle \langle \mathcal{L}_{21} \rangle}{\langle \mathcal{L}_{11} \rangle}, \tag{3.12b}$$

$$S = -\frac{\langle \mathcal{L}_{12} \rangle}{\langle \mathcal{L}_{11} \rangle}. \tag{3.12c}$$

Also, the Lorenz number L can be found from the Wiedemann-Franz law:

$$\frac{\kappa_e}{\sigma} = LT. \tag{3.13}$$

In essence, all thermoelectric quantities due to charge carriers can be obtained from evaluating the above integrals. The essential feature of these integrals is the tunneling integral function $M(\mathcal{E}_T, E)$ which is determined by the energy barrier in between the junction. The Fermi functions are decreasing functions of energy while $M(\mathcal{E}_T, E)$ is generally an overall increasing function of energy, not necessarily monotonic. Therefore, we expect the integrands of the integrals to be peaked functions of energy. The decreasing Fermi functions are weighted against the increasing $M(\mathcal{E}_T, E)$. If the Fermi functions decrease faster than $M(\mathcal{E}_T, E)$ increases, then tunneling is the dominant means of transport. If the Fermi functions decrease slower than $M(\mathcal{E}_T, E)$ increases, then thermal activation above the Fermi level is the dominant means of transport. For a general barrier with maximum φ_{max}, transport is then

divided into three regions (Fig. 8): tunneling below the Fermi level, tunneling of thermally activated electrons above the Fermi level but below φ_{max}, and thermal activation above φ_{max}. Low temperature transport is dominated by tunneling below the Fermi level and high temperature transport is dominated by thermal activation above φ_{max}. The intermediate temperature range where transport is determined mainly by tunneling of thermally activated electrons is relevant for a relatively small temperature range for reasonable barriers and will therefore be ignored. Low temperature and high temperature asymptotic forms of the responses will be obtained.

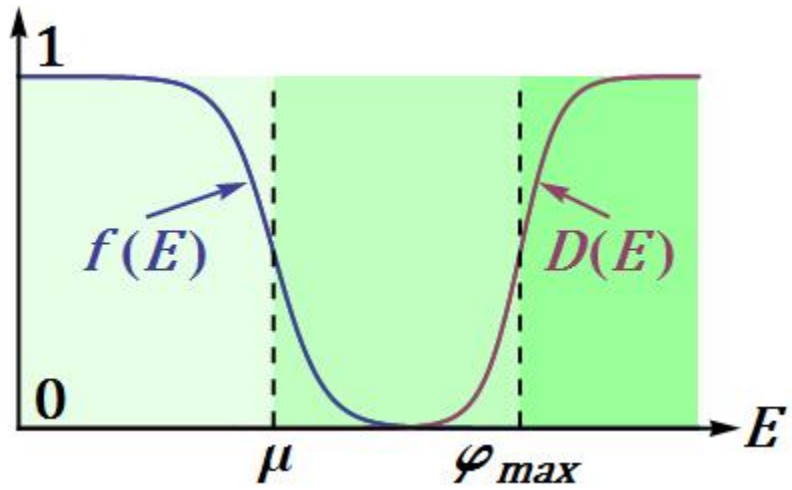

Figure 8. The Fermi function $f(E)$ and a representative tunneling probability $D(E)$ for the parabolic barrier as a function of energy. $f(E)$ decreases with energy whereas $D(E)$ increases with energy.

3.5 Effective-Medium Theory

All transport quantities have been described for a single junction. To develop these same transport quantities for a composite material, we will use an effective medium theory [57] since the composite material consists of many large conducting regions. We will assume the concentration of the composite material is well beyond the percolation threshold. In this theory, an inhomogeneous material is modeled as a homogeneous material with some "effective" microscopic transport quantities that can be related to the macroscopic transport quantities of the inhomogeneous material. Although effective medium theories have been developed for the conductivities of inhomogeneous systems [58, 59], we

will use an effective medium theory developed for an inhomogeneous system perturbed by both an electric field and temperature gradient [57].

In a composite material, each junction has some parameters, like the junction width. Across the entire material, there is a distribution of these parameters. From this distribution, effective medium theory uses a probability distribution for each junction parameter value across the network of junctions. The network, or composite, transport quantities are then found by averaging over these probability distributions. For example, if each junction were identical and had the same parameters, the probability distribution for the parameters would be a delta function. For this case, the network transport quantities are just those of a single junction.

Using the effective medium theory from [18], the current densities are given by

$$J = \sigma E + L_{12}\nabla T \quad , \quad J' = \sigma' E' + L'_{12}\nabla T' \tag{3.14a}$$
$$J^q = L_{21}E + L_{22}\nabla T \quad , \quad J^{q\prime} = L'_{21}E' + L'_{22}\nabla T', \tag{3.14b}$$

where the primed quantities refer to local quantities in the inhomogeneous material and unprimed quantities refer to the entire material.

It is found that

$$\langle \frac{\sigma' - \sigma}{\sigma' + 2\sigma} \rangle_{EMT} = 0 \quad \text{and} \quad \langle \frac{L'_{22} - L_{22}}{L'_{22} + 2L_{22}} \rangle_{EMT} = 0 \tag{3.15a}$$

and

$$\begin{aligned} L_{12} &= \sigma \langle \frac{L'_{12}}{(\sigma' + 2\sigma)(L'_{22} + 2L_{22})} \rangle_{EMT} \langle \frac{\sigma'}{(\sigma' + 2\sigma)(L'_{22} + 2L_{22})} \rangle_{EMT}^{-1} = \\ &= 3\sigma L_{22} \langle \frac{L'_{12}}{(\sigma' + 2\sigma)(L'_{22} + 2L_{22})} \rangle_{EMT} \langle \frac{\sigma' L_{22} + \sigma L'_{22} + 2\sigma L_{22} - \sigma' L'_{22}}{(\sigma' + 2\sigma)(L'_{22} + 2L_{22})} \rangle_{EMT}^{-1}, \end{aligned} \tag{3.15b}$$

$$\begin{aligned} L_{21} &= L_{22} \langle \frac{L'_{21}}{(\sigma' + 2\sigma)(L'_{22} + 2L_{22})} \rangle_{EMT} \langle \frac{L'_{22}}{(\sigma' + 2\sigma)(L'_{22} + 2L_{22})} \rangle_{EMT}^{-1} = \\ &= 3\sigma L_{22} \langle \frac{L'_{21}}{(\sigma' + 2\sigma)(L'_{22} + 2L_{22})} \rangle_{EMT} \langle \frac{\sigma' L_{22} + \sigma L'_{22} + 2\sigma L_{22} - \sigma' L'_{22}}{(\sigma' + 2\sigma)(L'_{22} + 2L_{22})} \rangle_{EMT}^{-1}. \end{aligned} \tag{3.15c}$$

The averaging is over all possible values of the junction parameters in the inhomogeneous system. Of course, the transport properties for the entire composite material are then defined in the usual way by

$$S = \frac{L_{12}}{\sigma} \quad \text{and} \quad \kappa = L_{22} - \frac{L_{12}L_{21}}{\sigma}. \tag{3.16}$$

A relationship for the thermopower S can also be found in terms of local thermopowers $S' = \frac{L'_{12}}{\sigma'}$,

$$S = 6L_{22}\frac{\langle S'D'\rangle_{EMT}}{1 - 3\langle L'_{22}D'\rangle_{EMT}} = \frac{\langle S'D'\rangle_{EMT}}{\langle D'\rangle_{EMT}}. \tag{3.17a}$$

Here,

$$D' = \frac{\sigma'}{(\sigma' + 2\sigma)(L'_{22} + 2L_{22})}. \tag{3.17b}$$

For the simple case considered here, we assume a delta distribution for the local quantities and then obtain

$$L_{11} = L'_{11}, \tag{3.18a}$$
$$L_{12} = L'_{12}, \tag{3.18b}$$
$$L_{21} = L'_{21}, \tag{3.18c}$$
$$L_{22} = L'_{22}. \tag{3.18d}$$

That is, the macroscopic quantities are just those for the local system, a single junction. In other words, all of our analysis for a single junction will give the same results for the composite polymer system.

4. RESULTS

4.1 Parabolic Barrier

As mentioned in the previous section, specification of the barrier in between the conducting regions is the only requirement to calculate the transport quantities. To this end, we will use the parabolic barrier as an example. The parabolic barrier is a simple barrier with an analytic expression for the tunneling probability and is also the barrier commonly used with fluctuation-induced tunneling.

We will use an extended parabolic barrier defined by

$$\varphi(\mathcal{E}_T, x) = 4\varphi_0 \frac{x}{w^2}(w - x) - qV_T \frac{(w - x)}{w} + \mu. \tag{3.19}$$

In this expression, $\varphi(\mathcal{E}_T, x)$ is the potential energy as a function of transverse distance x across the insulating junction between two conducting regions, $\varphi_0$is the parabolic barrier height, w is the width of the junction, $V_T = \mathcal{E}_T w$ is the potential difference between the two conducting regions due to a fluctuating field of strength $\mathcal{E}_T$, and μ is the unperturbed Fermi level of the conducting regions.

We will consider the parabolic barrier in three different ways. First, we will use the extended parabolic barrier case to find analytic approximations to the low temperature and high temperature transport quantities. Second, the extended parabolic barrier with no approximations will be used to find numerical results to show the behavior of the transport quantities and compare these results to the analytic approximations. Lastly, a truncated form of the parabolic barrier will be used. This form of the parabolic barrier differs from the extended barrier by truncating the barrier at the ends of the junction:

$$\varphi(\mathcal{E}_T, x) = \begin{cases} 4\varphi_0 \frac{x}{w^2}(w - x) - qV_T \frac{(w - x)}{w} + \mu, & 0 \le x \le w \\ -\infty & , \quad \text{otherwise} \end{cases}. \tag{3.20}$$

For the truncated parabolic barrier, a WKB approximation is used and transport properties are calculated numerically.

For the extended barrier, the exact tunneling probability is known [60,61],

$$D(\mathcal{E}_T, E) = \frac{1}{1 + e^{\frac{\gamma}{\varphi_0}(\varphi_{max} - E)}}, \tag{3.21a}$$

with

$$\gamma = \pi w \sqrt{\frac{m\varphi_0}{2\hbar^2}}. \tag{3.21b}$$

We explicitly find the tunneling integral

$$M(\mathcal{E}_T, E) = \frac{\varphi_0 qm}{\gamma \pi^2 \hbar^3} \mathrm{Log}\left[e^{\frac{\gamma}{\varphi_0}(E - \varphi_{max})} + 1\right]. \tag{3.22}$$

Although this is an exact expression for the tunneling integral, we approximate $M(\mathcal{E}_T, E)$ for analytic calculations as

$$M(\mathcal{E}_T, E) = \begin{cases} \frac{\varphi_0 em}{\gamma(2\pi)^2\hbar^3} e^{\frac{\gamma}{\varphi_0}(E - \varphi_{max})} & , \quad E < \varphi_{max} \\ \frac{em}{(2\pi)^2\hbar^3}(E - \varphi_{max}) & , \quad E > \varphi_{max} \end{cases}. \tag{3.23}$$

For low temperatures, a good approximation to the integrals is found using the Sommerfeld expansion. Using our approximation for $M(\mathcal{E}_T, E)$, it is seen that the Sommerfeld expansion is valid for $\frac{\varphi_0}{\gamma} > kT$, where tunneling dominates the transport. For $\frac{\varphi_0}{\gamma} < kT$, the dominant contribution to transport comes from thermal activation and the Sommerfeld expansion is not a good approximation because most of the transport occurs above the Fermi level. These two temperature regimes give rise to low temperature, $\frac{\varphi_0}{\gamma} > kT$, and high temperature, $\frac{\varphi_0}{\gamma} < kT$, behavior. We obtain asymptotic forms for the dominant terms in the linear responses for these two regimes.

4.2 Low Temperature and High Temperature Asymptotic Behavior

For the purpose of finding analytic approximations to $\mathcal{L}_{11} - \mathcal{L}_{22}$, we approximate the Fermi function as the Boltzmann distribution for large energies

$$f(E,T) = e^{-\frac{E-\mu}{kT}} \quad , \quad E > \mu, \tag{3.24a}$$

$$\frac{\partial f(E,T)}{\partial T} = \frac{(E-\mu)}{kT^2} e^{-\frac{E-\mu}{kT}} \quad , \quad E > \mu. \tag{3.24b}$$

In doing so, we find the high temperature approximations by integrating the energy from the Fermi level as a lower bound and ignore transport due to simple elastic tunneling.

4.3 Analytic Results

The analytic results for the low temperature and high temperature asymptotic behavior for the linear responses both in the presence and absence of thermal fluctuations are presented in Table 2.

The main parameters of the model refer to the junction: the width w of the junction, the surface area A of the junction, and the barrier height φ_0. Two other possible parameters are the permittivity ε_0 of the insulating region in the junction and the effective mass m of the charge carriers.

It should be noted that the low temperature conductivity in the presence of thermal fluctuations is what Sheng calculated in [43], found in Eq. (2.3). The main difference between what is shown in Table 2 and what is shown in Eq. (2.3) is the factor $\left(\frac{T_0}{T+T_0}\right)^{3/2}$. The reason for this difference is because of an assumption made in [43] that is not applicable to the extended parabolic barrier.

Table 2. The dominant low temperature and high temperature behaviors of the responses $\mathcal{L}_{11} - \mathcal{L}_{22}$ in the presence of thermal fluctuations and in the absence of thermal fluctuations as well as the temperature dependent conductivity σ, electronic thermal conductivity κ_e, thermopower S, and Lorenz number L in the low temperature and high temperature dominant terms both in the presence of thermal fluctuations and in the absence of thermal fluctuations. The effective parameters are the temperatures T_1 and T_0 and the dimensionless parameter α.

	Tunneling with Thermal Fluctuations	
	Low T	**High T**
$\langle \mathcal{L}_{11} \rangle$	$\frac{w\varphi_0 q^2 m}{2\gamma\pi^2\hbar^3}\left(\frac{T_0}{T+T_0}\right)^{3/2} e^{-\left(\frac{T_1}{T+T_0}\right)}$	$\frac{wq^2 m k_B}{2\pi^2\hbar^3}\left(\frac{\alpha}{1+\alpha}\right)^{3/2} T e^{-\frac{1}{T}\left(\frac{T_1}{1+\alpha}\right)}$
$\langle \mathcal{L}_{12} \rangle$	$\left(\frac{2wqmk_B^2}{6\hbar^3}\right)\left(T\sqrt{\frac{T_0}{T+T_0}}e^{-\left(\frac{T_1}{T+T_0}\right)}\right)$	$\frac{wqmk_B^2}{2\pi^2\hbar^3} T \left(\frac{\alpha}{1+\alpha}\right)^{1/2} e^{-\frac{1}{T}\left(\frac{T_1}{1+\alpha}\right)}\left(2+\frac{1}{2(1+\alpha)}\right)$
$\langle \mathcal{L}_{21} \rangle$	$\frac{w\varphi_0^2 qm}{\gamma\pi^2\hbar^3}\left(\frac{T}{T+T_0}\right)\left(\frac{T_0}{T+T_0}\right)^{3/2} e^{-\left(\frac{T_1}{T+T_0}\right)}$	$\frac{wqmk_B^2 T^2}{2\pi^2\hbar^3}\left(\frac{\alpha}{1+\alpha}\right)^{3/2} e^{-\frac{1}{T}\left(\frac{T_1}{1+\alpha}\right)}\left(2+\frac{3}{2(1+\alpha)}\right)$
$\langle \mathcal{L}_{22} \rangle$	$\left(\frac{w\varphi_0 mk_B^2}{6\gamma\hbar^3}\right)\left(T\sqrt{\frac{T_0}{T+T_0}}\left(1+\frac{2\gamma T}{(T+T_0)}\right)\right)e^{-\left(\frac{T_1}{T+T_0}\right)}$	$\frac{wmk_B^3 T^2}{8\pi^2\hbar^3}\frac{\alpha^{1/2} e^{-\frac{1}{T}\left(\frac{T_1}{1+\alpha}\right)}}{(1+\alpha)^{9/2}}(35+126\alpha+171\alpha^2+104\alpha^3+24\alpha^4)$
	Tunneling	
	Low T	**High T**
$\langle \mathcal{L}_{11} \rangle$	$\frac{w\varphi_0 q^2 m}{2\gamma\pi^2\hbar^3} e^{-\gamma}$	$\frac{wq^2 m}{2\pi^2\hbar^3} k_B T e^{-\gamma}$
$\langle \mathcal{L}_{12} \rangle$	$\frac{8wqm}{\pi^2\hbar^3} k_B^2 T e^{-\gamma}$	$\frac{wqm}{\pi^2\hbar^3} k_B^2 T e^{-\frac{V_0}{4kT}}$
$\langle \mathcal{L}_{21} \rangle$	$\frac{w\varphi_0 qm}{2\gamma\pi^2\hbar^3} k_B T e^{-\gamma}$	$\frac{wqm}{\pi^2\hbar^3} k_B^2 T^2 e^{-\frac{V_0}{4kT}}$
$\langle \mathcal{L}_{22} \rangle$	$\frac{2w\varphi_0 m}{\gamma\pi^2\hbar^3} k_B^2 T e^{-\gamma}$	$\frac{3wm}{\pi^2\hbar^3} k_B^3 T^2 e^{-\frac{V_0}{4kT}}$

	Tunneling with Thermal Fluctuations		**Tunneling**	
	Low T	**High T**	**Low T**	**High T**
σ	$\frac{w\varphi_0 q^2 m}{2\gamma\pi^2\hbar^3}\left(\frac{T_0}{T+T_0}\right)^{3/2} e^{-\left(\frac{T_1}{T+T_0}\right)}$	$\frac{wq^2 mk_B}{2\pi^2\hbar^3}\left(\frac{\alpha}{1+\alpha}\right)^{3/2} T e^{-\frac{1}{T}\left(\frac{T_1}{1+\alpha}\right)}$	$\frac{w\varphi_0 q^2 m}{2\gamma\pi^2\hbar^3} e^{-\gamma}$	$\frac{wq^2 mk_B}{\pi^2\hbar^3} T e^{-\frac{\varphi_0}{k_B T}}$
κ_e	$\left(\frac{w\varphi_0 mk_B^2}{6\gamma\hbar^3}\right) T\sqrt{\frac{T_0}{T+T_0}} e^{-\left(\frac{T_1}{T+T_0}\right)}$	$\frac{wmk_B^3}{\pi^2\hbar^3}\left(\frac{\alpha}{1+\alpha}\right)^{3/2} T^2 e^{-\frac{1}{T}\left(\frac{T_1}{1+\alpha}\right)}$	$\frac{w\varphi_0 mk_B^2}{6\gamma\hbar^3} T e^{-\gamma}$	$\frac{wmk_B^3}{\pi^2\hbar^3} T^2 e^{-\frac{\varphi_0}{k_B T}}$
S	$-\frac{\gamma\pi^2 k_B^2}{3q\varphi_0} T\left(1+\frac{T}{T_0}\right)$	$\frac{-2k_B}{q}\left(1+\frac{5}{4\alpha}\right)$	$-\frac{\gamma\pi^2 k_B^2}{3q\varphi_0} T$	$-\frac{2k_B}{q}$
L	$\frac{\pi^2 k_B^2}{3q^2}\left(1+\frac{T}{T_0}\right)$	$\frac{2k_B^2}{q^2}$	$\frac{\pi^2 k_B^2}{3q^2}$	$\frac{k_B^2}{q^2}$
Effective parameters		$T_1 = \frac{8\varepsilon_0\varphi_0^2 A}{k_B q^2 w}$	$T_0 = \frac{T_1}{\gamma}$	$\alpha = \frac{k_B T_1}{\varphi_0}$,

The low temperature and high temperature behavior of the transport quantities are drastically different. The only low temperature behavior that is nonmonotonic is found in σ in the presence of thermal fluctuations. All other low temperature and high temperature behaviors are monotonic in temperature. However, the overall temperature dependence of L is nonmonotonic and the same is generally true for S as well for a reasonable choice of parameters. The reason for this change in behavior is because of the transition from low temperature to high temperature behavior.

Lastly, the Lorenz number L deviates from the standard value $L = 2.44 \times 10^{-8}\ W\Omega/K^2$ given by the Wiedemann-Franz law. This indicates that the Wiedemann-Franz law is not entirely reliable for transport in conducting polymers. Deviations in the Lorenz number are not uncommon and can be observed in a variety of systems but the Lorenz number is often used to extract κ_e from the Wiedemann-Franz law. The model presented here allows extraction of κ_e using L from the model, knowing that L does not follow its standard value.

4.4 Temperature Dependence and Comparisons to Experimental Data

Fig. 9 shows the temperature dependence of the transport properties for the parabolic barrier. Panels (a) and (b) show comparisons to experimental data, while panels (c)-(h) show examples of different behaviors of the transport properties for different parameters. Panels (c), (e), and (g) show transport properties calculated with thermal fluctuations and panels (d), (f), and (h) show transport properties calculated without thermal fluctuations. The parameters used for the curves in Fig. 9 are found in Table 3.

A demonstration of the possible behaviors of the transport quantities as a function of temperature for the extended parabolic barrier is provided in Fig. 9, panels (c)-(h). The analytic approximations provided in Table 2 show a good comparison to the low temperature behavior. The charge q is chosen to signify holes as the charge carriers.

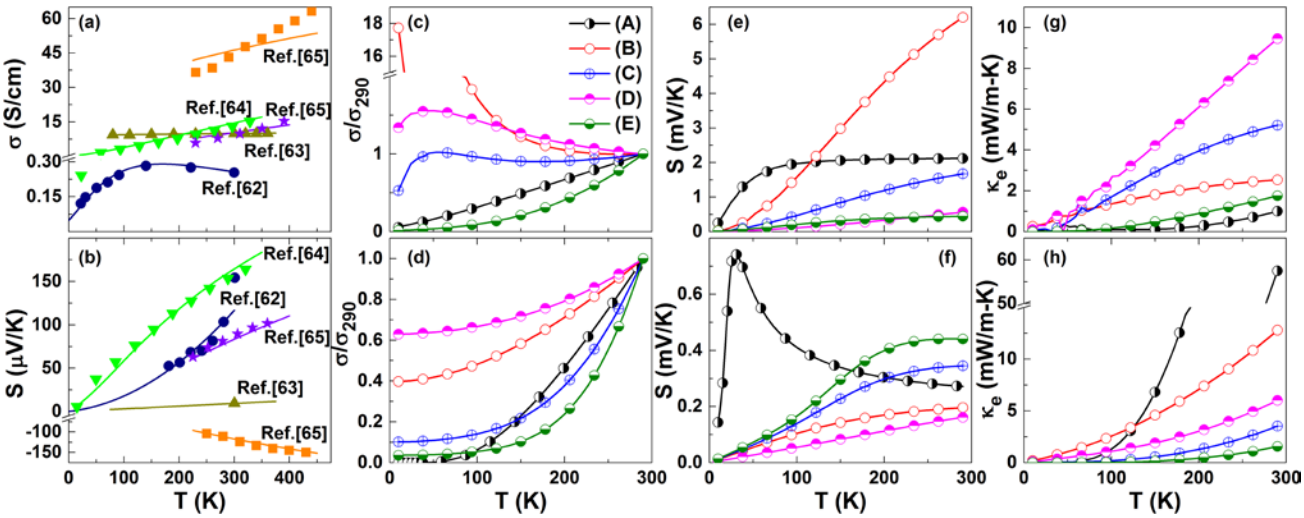

Figure 9. (a) and (b) show comparisons of the model to experimental data for the conductivity and thermopower. Symbols represent the experimental data and the solid lines correspond to the fitting. For the fit to Ref.[62], the low temperature results in the presence of thermal fluctuations for an extended parabolic barrier is used while Ref.[63], Ref.[64], and Ref.[65] use full numerical results (Eqs. (3.10a-d)) for a truncated parabolic barrier. Panels (c)-(h) show the temperature dependence of the conductivity, thermopower, and electronic thermal conductivity using Eqs. (3.10a-d) for an extended parabolic barrier. Curves for panels (c), (e), and (g) are calculated with thermal fluctuations and curves for panels (d), (f), and (h) are calculated without thermal fluctuations. The parameters used for all curves are shown in Table 3.

Table 3. The parameters used for the curves shown in Fig. 9.

	w (nm)	A (nm^2)	φ_0 (eV)	m/m_0		w (nm)	A (nm^2)	φ_0 (eV)	m/m_0
Ref.[62]	15.567	0.61841	1.32917	0.00127	**(A)**	7	70	0.025	1
Ref.[63]	2.39	5	0.375	0.008	**(B)**	1	2	0.025	1
Ref.[64]	2.5	1.7	0.3	1	**(C)**	2	4	0.1	1
Ref.[65]	1.38	2.5	0.055	0.82	**(D)**	1	2	0.125	1
Ref.[65]	1.05	1.3	0.425	0.8	**(E)**	2.5	50	0.125	1

With thermal fluctuations, the low temperature conductivity is a peaked function of temperature (Fig. 9c). The location, size, and width of this peak are controlled through the parameters. It is possible to push this peak into nonphysical negative temperatures so that the conductivity decreases with temperature (curve (B)). The conductivity in the absence of thermal fluctuations monotonically increases with temperature. Most other curves possess monotonic behavior, with the notable exception of S.

S is positive because holes are the charge carriers chosen. However, for data fitting, the sign of S is commonly indicative of the charge carriers and determines the sign of q. S generally increases

with low temperatures, but will eventually begin to decrease and saturate to the high temperature value. The transition from low temperature to high temperature behavior is apparent from the sharp peak of S for curve (A). All curves possess a similar behavior, but with broader, smaller peaks located at higher temperatures. The magnitude of S for the parameters chosen are closer to the values for lightly doped polymers, but can be adjusted (Fig. 9b).

κ_e has a monotonic temperature dependence for both tunneling in the presence and absence of thermal fluctuations. The main difference between curves for different parameters is the magnitude of κ_e. Using the Wiedemann-Franz law with a standard Lorenz number $L = 2.44 \times 10^{-8}\ W\Omega/K^2$, κ_e in the presence of thermal fluctuations is similar in magnitude to that of highly conducting polymers ($\sigma > 100\ S/cm$). Furthermore, κ_e is much smaller than κ of conducting polymers, indicating the dominant contribution κ_L from phonons to the thermal conductivity.

The model with a parabolic barrier is also used to fit experimental data (Fig. 9 panels (a) and (b)). The analytic expressions for the low temperature conductivity in the presence of thermal fluctuations is used to fit to [62] while numerical calculations for a truncated parabolic barrier are used to fit to the data in [63], [64], and [65]. The dark blue curve for data from [62] is for PEDOT:PSS samples formed from dispersions of 3-4% in water, the olive curve for data from [63] is for PEDOT:PSS samples drop-cast in water with 5% diethyelene glycol (DEG), the green curve for data from [64] is for semiconducting single-wall carbon nanotube (SWNT) films, the purple curve for data from [65] is for metal-coordinated poly(K_x[Ni-ett]), and the orange curve for data from [65] is for metal-coordinated poly(Cu_x[Cu-ett]). The fitting for the semiconducting SWNT film samples shows that this model is applicable to systems other than conductive polymers as well. As with the example curves also provided in Fig. 9, it is observed that the parabolic barrier is generally more suited for polymers with larger S. However, the model is flexible and accommodates doped polymers with a small S as well.

5. CONCLUSIONS

5.1 Summary and Outlook

Conducting polymers are environmentally friendly and cost-effective alternatives to inorganic materials for thermoelectric devices. The major drawback is their inherently low ZT as compared to inorganic thermoelectrics. Improving the conductivity and thermopower while simultaneously decreasing the thermal conductivity of conducting polymers will contribute to making conducting polymers competitive with inorganic thermoelectrics. To do so, a better understanding of the nature of charge transport in conducing polymers is needed, but our current understanding of transport processes in conducting polymers is lacking. There have been different models to describe the transport, with little focus on the fluctuation-induced tunneling model. For this model, only the conductivity has been examined. Here we provide a linear response theory for fluctuation-induced tunneling that allows for characterization of thermoelectric properties, including the conductivity, thermopower, and electronic thermal conductivity. The model is simple and only requires specification of the potential barrier in between the junctions of conducting regions in conducting polymers. We have used both the extended and truncated parabolic barriers with the model as examples. These barriers were used to fit experimental data of the conductivity and thermopower for several conducting polymers.

The model developed here could be used to help describe transport properties in conducting polymers. However, it is likely that the transport in conducting polymers is a combination of different mechanisms (like a combination of variable-range hopping and fluctuation-induced tunneling). Nonetheless, the model and results provided are applicable to disordered systems in general. To

improve upon the model, some example modifications include: the integration for the currents in (3.3a) and (3.3b) should be calculated using the bottom of the conduction band as a lower limit for E_x, different energy dispersions for the charge carriers can be used, alternative tunneling barriers should be explored, the inclusion of transport between different bands could be added, and the effects of interactions between charge carriers could be accounted for.

REFERENCES

[1] International Energy Agency, 2014, World Energy Outlook Factsheet, http://www.worldenergyoutlook.org/media/weowebsite/2014/141112_WEO_FactSheets.pdf.

[2] BP, 2014, BP Statistical Review of World Energy, http://www.bp.com/en/global/corporate/about-bp/energy-economics/statistical-review-of-world-energy.html.

[3] International Energy Agency, 2014, World Energy Investment Outlook, http://www.iea.org/publications/freepublications/publication/WEIO2014.pdf.

[4] Environmental Protection Agency, 2014, Inventory of U.S. Greenhouse Gas Emissions and Sinks: 1990-2012, http://www.epa.gov/climatechange/Downloads/ghgemissions/US-GHG-Inventory-2014-Main-Text.pdf.

[5] World Nuclear Association, 2014, http://www.world-nuclear.org/info/safety-and-security/safety-of-plants/safety-of-nuclear-power-reactors/ .

[6] T. J. Seebeck, Abh. K. Akad. Wiss. Berlin, 289 (1821).

[7] T. J. Seebeck, Abh. K. Akad. Wiss. Berlin, 265 (1823).

[8] T. J. Seebeck, Ann. Phys. (Lepizig)[2] **6**, 1 (1826).

[9] N. W. Ashcroft and N. D. Mermin, *Solid State Physics* (Brooks/Cole Cengage Learning, Belmont, 1976).

[10] J. C. A. Peltier, Ann. Chem. Phys. **56**, 371 (1849).

[11] E. J. Houston, *Electricity in Every-day Life* (P. F. Collier and Son, New York, 1905), Volume I.

[12] D. D. Pollock, *CRC Handbook of Thermoelectrics* edited by D. M. Rowe (CRC Press, Boca Raton, 1995), Section A.

[13] H. J. Goldsmid, *Introduction to Thermoelectricity* (Springer, Verlag Berlin Heidelberg, 2010).

[14] D. M. Rowe and C. M. Bhandari, *Modern Thermoelectrics* (Reston Publishing Company, Inc., Reston, 1983).

[15] P. M. Fishbane, S. G. Gasiorowicz, and S. T. Thornton, *Physics for Scientists and Engineers Third Edition* (Pearson Education Inc., Upper Saddle River, 2005), Volume I, Third Edition.

[16] F. Reiff, *Fundamentals of Statistical and Thermal Physics* (Waveland Press, Inc., Long Grove, 1965).

[17] G. L. Pollack and D. R. Stump, *Electromagnetism* (Addison Wesley, San Francisco, 2002), p.228-230.

[18] E. Altenkirch, Physik Z. **10**, 560 (1909).

[19] E. Altenkirch, Physik Z. **12**, 920 (1911).

[20] L. Dai, *Intelligent Macromolecules for Smart Devices: From Materials Synthesis to Device Applications* (Springer, London, 2004).

[21] W. D. Gill, W. Bludau, R. H. Geiss, P. M. Grand, R. L. Greene, J. J. Mayerle, and G. B. Street, Phys. Rev. Lett. **38**, 1305 (1977).
[22] C. K. Chiang, C. R. Fincher, Y. W. Park, A. J. Heeger, H. Shirakawa, E. J. Louis, S. C. Gau, and A. G. McDiarmid, Phys. Rev. Lett. **39**, 1098 (1977).
[23] O. Bubnova and X. Crispin, Energy Environ. Sci. **5**, 9345 (2012).
[24] C. K. Chiang, S. C. Gau, C. R. Fincher, Jr., Y. W. Park, A. G. MacDiarmid, and A. J. Heeger, App. Phys. Lett. **33**, 18 (1978).
[25] A. B. Kaiser, Rep. Prog. Phys. **64**, 1 (2001).
[26] A. J. Heeger, J. Phys. Chem. B **105**, 8475 (2001).
[27] H. Shirakawa, Angew. Chem. Int. Ed. **40**, 2574 (2001).
[28] A. G. MacDiarmid, Angew. Chem. Int. Ed. **40**, 2581 (2001).
[29] A. B. Kaiser, Adv. Mater. **13**, 927 (2001).
[30] N. Dubey and M. Leclerc, J. Polym. Sci., Part B: Poym. Phys. **49**, 467 (2011).
[31] T. O. Poehler and H. E. Katz, Energy Environ. Sci. **5**, 8110 (2012).
[32] E. B. Park, J. S. Yoo, J. Y. Park, Y. W. Park, K. Akagi, and H. Shirakawa, Synt. Met. **69**, 61 (1995).
[33] K. K. Lee, A. S. Alexandrov, and W. Y. Liang, Phys. Rev. Lett. **90**, 217001 (2003).
[34] Y. Du, S. Z. Shen, K. Cai, and P. S. Casey, Prog. Polym. Sci. **37**, 820 (2012).
[35] O. Bubnova, Z. U. Khan, A. Malti, S. Braun, M. Fahlman, M. Berggren, and X. Crispin, Nat. Mater. **10**, 429 (2011).
[36] G. H. Kim, L. Shao, K. Zhang, and K. P. Pipe, Nat. Mater. **12**, 719 (2013).
[37] B. Poudel, Q. Hao, Y. Ma, Y. Lan, A. Minnich, B. Yu, X. Yan, D. Wang, A. Muto, D. Vashaee, X. Chen, J. Liu, M. S. Dresselhaus, G. Chen, and Z. Ren, Science **320**, 634 (2008).
[38] J. L. Brédas and G. B. Street, Acc. Chem. Res. **18**, 309 (1985).
[39] H. S. Nalwa, *Handbook of Advanced Electronic and Photonic Materials and Devices* (Academic Press, San Diego, 2001).
[40] D. Emin, Phys. Rev. B. **53**, 1260 (1996).
[41] N. F. Mott and E. A. Davis, *Electronic Processes in Non-Crystalline Materials, 2nd ed.* (Clarenton, Oxford, 1979).
[42] H. Overhof, Phys. Stat. Sol. B **67**, 709 (1975).
[43] P. Sheng, Phys. Rev. B **21**, 2180 (1980).
[44] A. B. Kaiser and V. Skákalova, Chem. Soc. Rev. **40**, 3786 (2011).
[45] E. K. Sichel, P. Sheng, J. I. Gittleman, and S. Bozowski, Phys. Rev. B **24**, 6131 (1981).
[46] J. Ederth, P. Johnsson, G. A. Niklasson, A. Hoel, A. Hultåker, P. Heszler, C. G. Granqvist, A. R. van Doorn, M. J. Jongerius, and D. Burgard, Phys. Rev. B **68**, 155410 (2003).
[47] S. Mitra, S. Banerjee, and D. Chakravorty, J. Appl. Phys. **113**, 154314 (2013).
[48] J. Syurik, O. A. Ageev, D. I. Cherednichenko, B. G. Konoplev, and A. Alexeev, Carbon **63**, 317 (2013).
[49] M. Salvato, M. Cirillo, M. Lucci, S. Orlanducci, I. Ottaviani, M. L. Terranova, and F. Toschi, Phys. Rev. Lett. **101**, 246804 (2008).
[50] R. J. Cohen and A. J. Glick, Phys. Rev. B **46**, 1564 (1992).
[51] S. Paschen, M. N. Bussac, L. Zuppiroli, E. Minder, and B. Hilti, J. Appl. Phys. **78**, 3230 (1995).
[52] G. C. McIntosh and A. B. Kaiser, Curr. Appl. Phys. **1**, 145 (2001).

[53] H. Xie and P. Sheng, Phys. Rev. B **79**, 165419 (2009).
[54] I. V. Krive, E. N. Bogachek, A. G. Scherbakov, and U. Landman, Phys. Rev. B **64**, 23304 (2001).
[55] Y. V. Nazarov and Y. M. Blanter, *Quantum Transport: Introduction to Nanoscience* (Cambridge University Press, Cambridge, 2009).
[56] K. Hansen and M. Brandbyge, J. Appl. Phys **95**, 3582 (2004).
[57] I. Webman, J. Jortner, and M. Cohen, Phys. Rev. B **16**, 2959 (1977).
[58] S. Kirkpatrick, Rev. Mod. Phys. **45**, 574 (1973).
[59] J. Bernasconi, Phys. Rev. B **7**, 2252 (1973).
[60] E. C. Kemble, *The Fundamental Principles of Quantum Mechanics with Elementary Applications* (McGraw-Hill, New York, 1937), p. 109.
[61] L. D. Landau and E. M. Lifshitz, *Quantum Mechanics. Non-Relativistic Theory* (Pergamon Press, Oxford, 1977).
[62] Our paper to be submitted (G. S. Nolas data).
[63] O. Bubnova, Z. U. Khan, H. Wang, S. Braun, D. R. Evans, M. Fabretto, P. Hojati-Talemi, D. Dagnelund, J.-B. Arlin, Y. H. Geerts, S. Desbief, D. W. Breiby, J. W. Andreasen, R. Lazzaroni, W. M. Chen, I. Zozoulenko, M. Fahlman, P. J. Murphy, M. Berggren, and X. Crispin, Nat. Mater. **13**, 190 (2014).
[64] Y. Nakai, K. Honda, K. Yanagi, H. Kataura, T. Kato, T. Yamamoto, and Y. Maniwa, App. Phys. Lett. **7**, 025103 (2014).
[65] J. Yang, H. Yip, and A. K.-Y. Jen, Adv. Energy Mater. **3**, 549 (2013).